Measurement of Stokes parameters

Bachelorarbeit
von

Prokhor Tkhor

am FZ Jülich PGI-9

Reviewer:	Prof. Dr. B. Kardynal
Second Reviewer:	Prof. Dr. T. Taubner

Bearbeitungszeit: 01.04.2019 – 01.11.2019

Contents

List of Figures

List of Tables

1. Introduction

1.1 Introduction

Polarization of light has a vast array of applications in our daily lives, from polarization filters in sunglasses and photography [1], [2] over the LCD technology in displays [3] to radio antennas [4]. It helped facilitate a number of scientific discoveries [5], especially in astronomy [6].

The first polarimeter was designed by Biot in 1848 to analyze the optical activity of tartaric acids [7]. Since then polarimetry has gone a long way and today highly specialized commercial products are available.

Polarimeters are widely used in astrophysical observatories e.g. they can be used to analyze the magnetic field of galaxies or cosmic dust, which plays an important role in the formation of stars[8].

Today polarimetry, as the measurement of polarization is referred to, plays an important role in many fields of physics. It can be used to characterize single-layer materials such as WSe_2 or MoS_2. When excited with laser light electron-hole pairs known as excitons form between the valence and conduction bands. The light emitted from their decay depends on the polarization of the exciting light.[9].

The reason why one can not easily use the commercial polarimeter (Thorlabs TXP Polarimeter PAX5720IR1-T) available for measurements of 2D materials is that it analyzes the total intensity and has no spectral resolution. The method previously used for polarization measurements by us involves modulating the polarization by means of rotating the fast axes of a quarterwave-plate and a halfwave-plate manually to specific angles and comparing the transmitted intensity through a linear polarizer for the different angles. This requires a lot of manual labor and is not always feasible during an experiment.

Therefore, the aim for this thesis is to construct an automated polarimeter from a linear polarizer and a rotating quarter-waveplate with the optical components chosen such that we are able to conduct polarization measurements quickly for the photoluminescence signal of WSe_2 and MoS_2 monolayers. Consequently, the automated system was tested on different pre-configured polarizations of laser light to find error sources and estimate the accuracy of the polarization results. For that the characteristics of the optical components in use had to be determined. Also, a routine for extracting the polarization parameters from the measured intensity was written. Lastly, a monolayer of WSe_2 was excited with laser light of different polarizations. The decay was captured as photoluminescence spectra and the different excitonic species were subjected to a polarimetric analysis using the developed setup.

2. Theoretical Background

The aim of this introductory chapter is to remind the reader of the basic concepts of electromagnetic waves and polarization of light, which can be described by Stokes vectors and illustrated on the Poincaré sphere. Also, two methods of describing the effects of optical elements on light called Müller and Jones calculus are explained. Further, three different methods of measuring the Stokes vectors are discussed in detail, as the results obtained from these methods are the main part of this thesis.

2.1 Polarization of light

Light is an electromagnetic wave, whose electric ($\vec{E}$) and magnetic ($\vec{H}$) fields can be described by Maxwell's equations with charge density ρ, current density $\vec{j}$, vacuum permittivity ϵ_0 and vacuum permeability μ_0:

$$\begin{aligned} \vec{\nabla} \cdot \vec{E}(\vec{x},t) &= \frac{\rho(\vec{x},t)}{\epsilon_0} \\ \vec{\nabla} \cdot \vec{B}(\vec{x},t) &= 0 \\ \vec{\nabla} \times \vec{E}(\vec{x},t) &= -\frac{\partial \vec{B}(\vec{x},t)}{\partial t} \\ \vec{\nabla} \times \vec{B}(\vec{x},t) &= \mu_0 \vec{j}(\vec{x},t) + \mu_0 \epsilon_0 \frac{\partial \vec{E}(\vec{x},t)}{\partial t} \end{aligned} \tag{2.1}$$

In vacuum wave equations can be derived from these relations:

$$\begin{aligned} \Delta \vec{E}(\vec{x},t) &= \mu_0 \epsilon_0 \frac{\partial^2 \vec{E}(\vec{x},t)}{\partial t^2} \\ \Delta \vec{B}(\vec{x},t) &= \mu_0 \epsilon_0 \frac{\partial^2 \vec{B}(\vec{x},t)}{\partial t^2} \end{aligned} \tag{2.2}$$

The wave equations for light propagating in z-direction are solved by plane waves of the form

$$\vec{E}(z,t) = \underbrace{E_x sin(\omega t - kz)}_{a_x} \vec{e}_x + \underbrace{E_y sin(\omega t - kz + \phi)}_{a_y} \vec{e}_y \tag{2.3}$$

with angular frequency of the light ω, wavenumber k, absolute values of orthogonal electric field components E_x and E_y, instantaneous electric field components a_x, a_y and phase difference between the two directions ϕ.

While any linear superposition of waves of the form eq. (2.3) solves eq. (2.2), special cases of light where the electric field oscillates in only one direction or is rotated around the optical axis can be defined. We call such light linearly or elliptically polarized light, respectively. Depending on E_x, E_y and ϕ we differentiate between several types of polarization, as seen in Tab. 2.1.

E_x	E_y	ϕ [rad]	Polarization
1	0	—	horizontal linear polarization
1	1	0	diagonal linear polarization
0	1	—	vertical linear polarization
1	1	π	antidiagonal linear polarization
1	1	$\frac{\pi}{2}$	right-handed circular polarization
1	1	$-\frac{\pi}{2}$	left-handed circular polarization

Table 2.1: Different types of polarization in dependance of the electric field amplitudes E_x, E_y and phase difference ϕ

Polarized light can be described conveniently by introducing the Poincaré-sphere, see Fig. 2.1, where each point on the unit sphere corresponds to a different polarization state. Points within the Poincaré-sphere correspond to different degrees of polarization (DOP), which describes the ratio between polarized and unpolarized components of an electromagnetic wave. Therefore, each polarization state can be expressed in spherical coordinates. The point H stands for horizontal polarization and the opposite point on the equator V for vertical polarization.

In general the polarization of light can be described by the three parameters λ, $\tilde{\omega}$ and DOP as shown in Fig. 2.2. Depending on whether the point P is in the upper or lower hemisphere, the light beam has left- or right-handedness.

2.2 Stokes vectors and Müller calculus

In order to describe the polarization of light within the Poincare sphere it is convenient to define the so called Stokes vector, which consists of four entries

$$I =< a_x^2 + a_y^2 > \tag{2.4}$$
$$M =< a_x^2 - a_y^2 > \tag{2.5}$$
$$C =< 2a_x a_y cos\phi > \tag{2.6}$$
$$S =< 2a_x a_y sin\phi > \tag{2.7}$$
$$\tag{2.8}$$

$a_x = E_x sin(\omega t - kz)$ and $a_y = E_y sin(\omega t - kz + \phi)$ are the instantaneous amplitudes of the electric field vectors in x- and y-direction, with ϕ being their phase difference. The angular brackets are denoting temporal averaging with the averaging interval being at least one oscillation period. I is the total intensity, M, C and S can assume values between -1 and 1. They describe the polarization of light, with M indicating horizontal or vertical polarization, C indicating linear polarization in the bases rotated by an 45° angle and S indicating left- or right-handed circularly polarized light.

Using Müller calculus one can easily calculate the effect of an optical device on a polarized light beam by multiplying its Stokes vector from right by the 4x4 Müller-matrices, which describe the particular optical elements. Its general form is

$$\begin{bmatrix} I' \\ M' \\ C' \\ S' \end{bmatrix} = \begin{bmatrix} m_{11} & m_{12} & m_{13} & m_{14} \\ m_{21} & m_{22} & m_{23} & m_{24} \\ m_{31} & m_{32} & m_{33} & m_{34} \\ m_{41} & m_{42} & m_{43} & m_{44} \end{bmatrix} \begin{bmatrix} I \\ M \\ C \\ S \end{bmatrix}$$

with the primed Stokes vector being defined as the polarization of the light beam behind the optical element and the non-primed as the initial polarization. To compute the beam

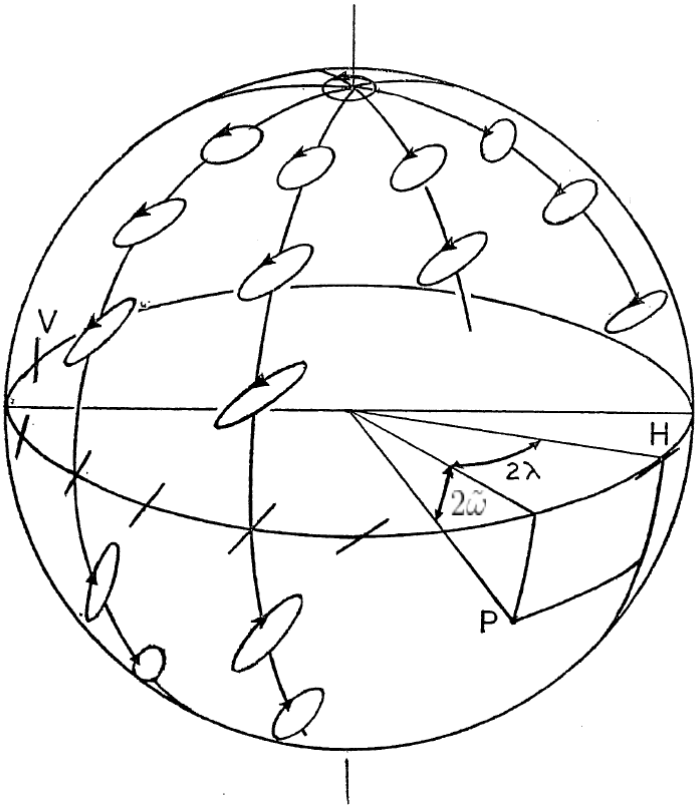

Figure 2.1: Poincaré Sphere. The Point P is determined by an azimuthal angle 2λ and a polar angle of $2\tilde{\omega}$ from a point H on the equator, taken from [10]

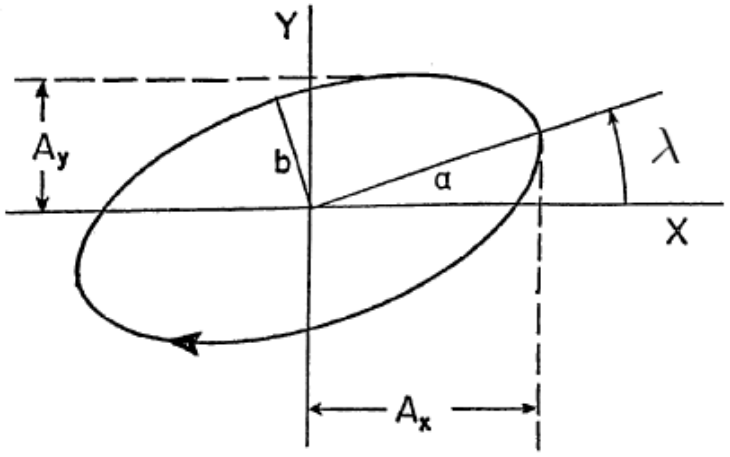

Figure 2.2: Sectional pattern. λ corresponds to the azimuth, a to the major axis, b to the minor axis, and $\tan\tilde{\omega} = \frac{b}{a}$ to the ellipticity of the ellipse, taken from [10]

which passes through a succession of optical devices it is sufficient to multiply their Müller matrices in the correct order to the Stokes vector of the incident light. Although for many optical elements the ideal Müller matrix is known, the right parameters of the individual Müller matrices for real optical devices are found phenomenologically by experimentation [10].

In order to obtain the Müller matrix P_Θ of a device rotated by an azimuthal angle of Θ around the optical axis, rotation matrices $T(\Theta)$ are applied to the Müller matrix of the device P_0 with rotation angle $\lambda = 0$

$$[P_\Theta] = [T(-\Theta)]\,[P_0]\,[T(\Theta)] \tag{2.9}$$

with

$$[T(\Theta)] = \begin{bmatrix} 1 & 0 & 0 & 0 \\ 0 & cos2\Theta & -sin2\Theta & 0 \\ 0 & sin2\Theta & cos2\Theta & 0 \\ 0 & 0 & 0 & 1 \end{bmatrix} \tag{2.10}$$

The Müller-matrix for an ideal half-waveplate with horizontal fast axis is

$$\left[\frac{\lambda}{2}\right] = \begin{bmatrix} 1 & 0 & 0 & 0 \\ 0 & 1 & 0 & 0 \\ 0 & 0 & -1 & 0 \\ 0 & 0 & 0 & -1 \end{bmatrix} \tag{2.11}$$

, for a quarter-waveplate with horizontal fast axis[10]

$$\left[\frac{\lambda}{4}\right] = \begin{bmatrix} 1 & 0 & 0 & 0 \\ 0 & 1 & 0 & 0 \\ 0 & 0 & 0 & 1 \\ 0 & 0 & -1 & 0 \end{bmatrix} \tag{2.12}$$

and for a linear polarizer with horizontal transmission axis

$$[Pol] = \frac{1}{2}\begin{bmatrix} 1 & 1 & 0 & 0 \\ 1 & 1 & 0 & 0 \\ 0 & 0 & 0 & 0 \\ 0 & 0 & 0 & 0 \end{bmatrix} \tag{2.13}$$

2.3 Jones vectors and Jones calculus

In addition to the Stokes formalism, the polarization of light can be described in the Jones formalism. To use the Jones calculus one needs to define the Jones vector first, which characterizes a polarized beam and consists of two entries - the complex electric field in x- and in y-direction:

$$\vec{J} = \begin{bmatrix} E_{x_0} e^{i\phi_x} \\ E_{y_0} e^{i\phi_y} \end{bmatrix} \tag{2.14}$$

For example

$$\vec{J}_H = \begin{bmatrix} E_{x_0} e^{i\phi_x} \\ 0 \end{bmatrix} \tag{2.15}$$

is horizontally linearly polarized light and

$$\vec{J}_{RC} = \begin{bmatrix} E_{x_0} e^{i\phi_x} \\ E_{x_0} e^{i(\phi_x + \frac{\pi}{2})} \end{bmatrix} \tag{2.16}$$

is right-handed circularly polarized light.

The Jones vector can be normalized and used together with 2x2 Jones-matrices, which work in a similar fashion to the Müller-Calculus to calculate the resulting form of the polarized vector after it is subjected to the optical devices. In order to obtain the Jones matrix M_Θ of a device rotated by an azimuthal angle of Θ around the optical axis, rotation matrices $R(\Theta)$ are applied to the Jones matrix M_0 of the device with rotation angle $\lambda = 0$

$$[M_\Theta] = [R(\Theta)]\,[M_0]\,[R(-\Theta)] \tag{2.17}$$

with

$$R_\Theta = \begin{bmatrix} cos(\Theta) & -sin(\Theta) \\ sin(\Theta) & cos(\Theta) \end{bmatrix}$$

The Jones matrix for a quarter-wave plate with horizontal fast axis is

$$M_{\lambda/4} = e^{-i\frac{\pi}{4}} \begin{bmatrix} 1 & 0 \\ 0 & i \end{bmatrix}$$

, for a half-wave plate with horizontal fast axis

$$M_{\lambda/2} = -i \begin{bmatrix} 1 & 0 \\ 0 & i \end{bmatrix}$$

and for a linear polarizer with horizontal transmission axis

$$M_{LP} = \begin{bmatrix} 1 & 0 \\ 0 & 0 \end{bmatrix}$$

2.4 Comparing Müller and Jones Calculus

The Müller and Jones calculus have much in common, namely they both employ a standardized matrix algebra method to calculate the effects of multiple optical elements. However, there are also some striking differences between the two formalisms. For instance Müller calculus is suited to treat depolarizing elements unlike Jones calculus. In return Jones calculus retains the absolute phase of a light beam and is able to handle interference of two coherent light beams[10].

2.5 Measuring Stokes vectors using two retarders and a polarizer

We take an arbitrary polarized light beam expressed through a Jones vector

$$|In\rangle = \begin{bmatrix} E_{x_0} e^{i\phi_x} \\ E_{y_0} e^{i\phi_y} \end{bmatrix} = \begin{bmatrix} a \\ b \end{bmatrix} \tag{2.18}$$

and pass the light through a quarter-wave-plate, a half-wave-plate and a linear polarizer. The concept is based on a fixed linear polarizer and the set of waveplates being able to assume different angles making it a variable retarder. The $\frac{\lambda}{4}$-waveplate is placed at variable angles, which in combination with the linear polarizer makes the circular and linear intensity

components of the light accessible for measurement. Between $\frac{\lambda}{4}$-waveplate and the linear polarizer a $\frac{\lambda}{2}$-waveplate is placed at specific angles in order to be able to measure the orthogonal components to the horizontal, diagonal, and right-circular polarizations.

For example the resulting Jones vector $|Out\rangle$ of a light beam traveling through a combination of $\lambda/4$-plate at 45° and $\lambda/2$-plate at 22.5° and linear polarizer at 0° can be obtained by

$$|Out\rangle = \boldsymbol{M_{LP}M_{\lambda/2}M_{\lambda/4}}\,|In\rangle = \begin{pmatrix}1 & 0\\ 0 & 0\end{pmatrix}\frac{1}{\sqrt{2}}\begin{pmatrix}1 & 1\\ 1 & -1\end{pmatrix}\frac{\exp^{i\pi/4}}{2}\begin{pmatrix}1+i & (1-i)\\ (1-i) & 1+i\end{pmatrix}|In\rangle$$
$$= \begin{pmatrix}a(1+i)+b(1+i)\\ 0\end{pmatrix}$$

, which gives access to the diagonal component $|D\rangle$ of the incident light $|In\rangle$

The difference between linear and circular orthogonal components yields the Stokes parameters. There are six different settings of the retarders axes, which need to be set up in order to measure the whole set of Stokes parameters. The used settings are listed in Table 2.2.

Input	$\lambda/4$	$\lambda/2$	LP	Output	Tested component
(a,b)	0°	0°	0°	a	$\|H\rangle$
(a,b)	0°	45°	0°	b	$\|V\rangle$
(a,b)	45°	22.5°	0°	(a+b)(1+i)	$\|D\rangle$
(a,b)	45°	−22.5°	0°	(b-a)(1-i)	$\|A\rangle$
(a,b)	45°	0°	0°	b+ia	$\|R\rangle$
(a,b)	−45°	0°	0°	-b+ia	$\|L\rangle$

Table 2.2: Combinations of angles set with the waveplates to return specific polarizations

The total intensity is calculated by addition of the measured orthogonal components

$$I = H + V = D + A = R + L = a + b \tag{2.19}$$

and the other entries of the Stokes vector by subtracting the measured components

$$M = H - V \tag{2.20}$$
$$C = D - A \tag{2.21}$$
$$S = R - L \tag{2.22}$$

The advantage of this method is that it is straight-forward and depending on the skill of the experimenter fast, but to be precise we need to calibrate the angles of the optical components with respect to the reference plane for each of the measurement settings mentioned in Tab. 2.2. Also, the precise adjustment of the angles of the optical components by the experimenter is tedious and in case of experiments highly sensitive to light difficult to execute in the dark. Another disadvantage is that automatization of this method would require two controllable rotating stages.

2.6 Measuring Stokes vectors using one retarder and a polarizer

In addition to the technique explained in section 2.6 the polarization of light can be measured using only one retarder and a linear polarizer. The setup is shown in Fig. 2.3. In general we calculate the emerging Stokes vector by using Müller calculus [11], where we

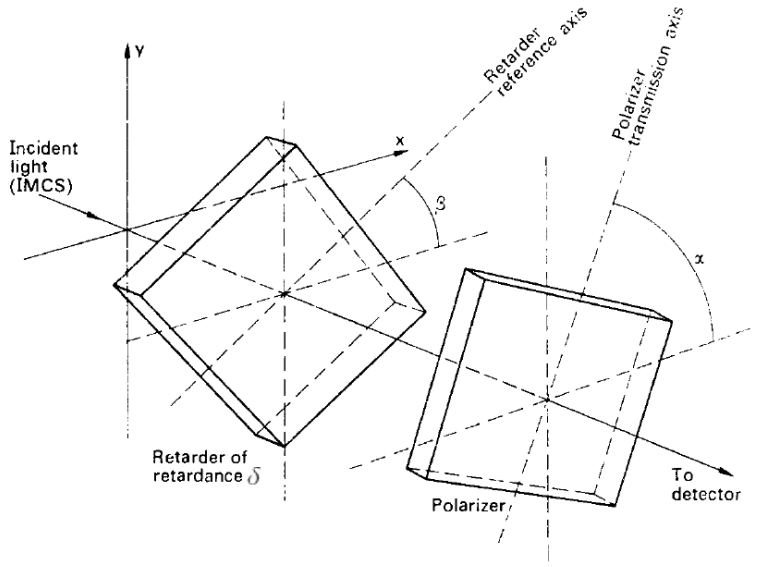

Figure 2.3: Polarimetric arrangement, consisting of a retarder with retardance δ and its fast axis with angle β to the x-axis and a polarizer with the transmitting axis in angle α to the x-axis, taken from [11]

have

$$\begin{bmatrix} I'^* \\ M'^* \\ C'^* \\ S'^* \end{bmatrix} = [Pol]\,[T(2(\alpha-\beta))]\,[\Delta]\,[T(2\beta)] \begin{bmatrix} I \\ M \\ C \\ S \end{bmatrix}$$

with

$$[\Delta] = \begin{bmatrix} 1 & 0 & 0 & 0 \\ 0 & 1 & 0 & 0 \\ 0 & 0 & cos\delta & sin\delta \\ 0 & 0 & -sin\delta & cos\delta \end{bmatrix} \tag{2.23}$$

being the effect of the retarder with retardance δ. Eq. (2.10) is used to go from the retarders to the polarizers reference frame. Lastly, with eq. (2.13) we take the effect of the linear polarizer [Pol] into account.

Thus, we obtain

$$I'^*(\alpha,\beta,\delta) = \frac{1}{2}\{I\,[Mcos2\beta + Csin2\beta]\,cos2(\alpha-\beta) + [(Ccos2\beta - Msin2\beta)cos\delta + Ssin\delta]\,sin2(\alpha-\beta)\} \tag{2.24}$$

In order to use the technique with the rotating retarder plate, we need to calibrate our retardance δ, as the resulting intensity depends on it. For this purpose we use two linear polarizers P_1 and P_2 of which the first is rotatable and the other is at a fixed angle α. By rotating the first linear polarizer we find two angles where the transmitted intensity is maximal and minimal, which we use to calculate the efficiency of P_1

$$\frac{M}{I}(\lambda) = k_{inc}(\lambda) = \frac{I_{max} - I_{min}}{I_{max} + I_{min}} \tag{2.25}$$

Now we can reinsert the retardation plate to obtain the phase shift

$$\delta(\lambda) = arccos(\frac{1 - |\eta| cos2\alpha - 2\frac{|\eta|}{k_{inc}(\lambda)}}{1 + |\eta| cos2\alpha}) \tag{2.26}$$

α can be obtained by setting up horizontal polarization for the incoming light beam and adjusting the linear polarizer to show maximum transmission, which corresponds to $\alpha = 0$. The modulation ratio $|\eta|$ is determined from the transmitted intensity while the retarder is rotated between the linear polarizers.

$$\eta = \frac{I_{max} - I_{min}}{I_{max} + I_{min}} = \frac{M(1 - cos\delta)}{2I + Mcos2\alpha(1 + cos\delta)} \tag{2.27}$$

After calibration of the retardance δ the quarter-waveplate is rotated by small angular steps of $\Delta\beta$. We rewrite our transmitted intensity to

$$\begin{aligned} I_T(\alpha, \beta, \delta) = \frac{1}{2}\left[I + \left(\frac{M}{2}cos2\alpha + \frac{C}{2}sin2\alpha\right)(1 + cos\delta)\right] + \frac{1}{2}\left[Ssin\beta \cdot sin2(\alpha - \beta)\right] \\ + \frac{1}{4}\left[(Mcos2\alpha - Csin2\alpha)cos4\beta + (Msin2\alpha + Ccos2\alpha)sin4\beta\right](1 - cos\beta) \end{aligned} \tag{2.28}$$

and recognize that it can be represented as a Fourier series

$$I_T(\beta) = C_0 + C_2 cos2\beta + C_4 cos4\beta + S_2 sin2\beta + S_4 sin4\beta \tag{2.29}$$

After gathering N=2L data points,we calculate the Fourier series coefficients with

$$C_{\omega_k} = \frac{2}{N}\frac{1}{1 + \delta_{k0} + \delta_{kL}}\sum_{i=1}^{N} I_{T_i} cos\omega_k\beta_i \tag{2.30}$$

$$S_{\omega_k} = \frac{2}{N}\frac{1}{1 + \delta_{k0} + \delta_{kL}}\sum_{i=1}^{N} I_{T_i} sin\omega_k\beta_i \tag{2.31}$$

where k =0,1..L, Kronecker delta δ_{ij} and

$$\omega_k = \frac{2\pi}{N}\frac{k}{\Delta\beta} \tag{2.32}$$

These coefficients equal zero, except for the cases where ω_k= 2 or 4. When choosing the step size $\Delta\beta$ and the number of data points we need to consider that ω_k= 2, 4 must be included, as we calculate the important Fourier coefficients from these frequencies.

After identifying the prefactors of the sine and cosine terms with the Fourier coefficients, we get expressions for the Stokes parameters

$$M = \frac{2}{1 - cos\delta}\left[C_4 cos(2\alpha + 4\beta_0) + S_4 sin(2\alpha + 4\beta_0)\right] \tag{2.33}$$

$$C = \frac{2}{1 - cos\delta}\left[S_4 cos(2\alpha + 4\beta_0) - C_4 sin(2\alpha + 4\beta_0)\right] \tag{2.34}$$

$$S = \frac{C_2}{sin\delta sin(2\alpha + 4\beta_0)} = \frac{-S_2}{sin\delta cos(2\alpha + 4\beta_0)} \tag{2.35}$$

$$|S| = \frac{(C_2^2 + S_2^2)^{\frac{1}{2}}}{sin^2\delta} \tag{2.36}$$

$$I = C_0 - \frac{1 + cos\delta}{1 - cos\delta}\left[C_4 cos(4\alpha + 4\beta_0) + S_4 sin(4\alpha + 4\beta_0)\right] \tag{2.37}$$

Additionally we can calculate |M| from

$$|M| = \frac{1}{1 - cos\delta} \times (C_4^2 + S_4^2)^{\frac{1}{2}} \tag{2.38}$$

for the case that C,S = 0, which means that the light from the source is horizontally polarized.

In order to obtain the values of the parameters we need to measure the angles α of the linear polarizer and β_0 of the retarder in relation to the reference plane. For α this can be done while setting the system up using the method described in the previous paragraph and β_0 can be obtained by measuring either strongly circularly polarized light or strongly linearly polarized light and using the relations below.

For strongly circularly polarized light we get

$$tan(4\beta_0 + 2\alpha) = \frac{-C_2}{S_2} \tag{2.39}$$

and for strongly linearly polarized light with C=S=0 we get

$$tan(4\beta_0 + 2\alpha) = \frac{S_4}{C_4} \tag{2.40}$$

2.7 Self-calibrating polarimetric method using one retarder and a polarizer

An alternative method for polarization measurement by Andreev [12] will be introduced, because the angles of the transmission axis of the linear polarizer and the retarders fast axis need to be calibrated precisely.

The setup is calibrated by doing two measurements on horizontally-polarized light with the linear polarizer being in position $\alpha_0 = 0°$ for the first and $\alpha_0 = 45°$ for the second measurement and using the Fourier coefficients from both measurements to simplify the equations (2.33)-(2.37), as $cos(\delta) \backsimeq \frac{\pi}{2} - \delta$, which corresponds to a $\frac{\lambda}{4}$-waveplate

$$\delta = \frac{\pi}{2} + 1 + 2\frac{\sqrt{C_4^2 + S_4^2} - C_0}{\sqrt{C_4^2 + S_4^2} + C_0} \tag{2.41}$$

$$\alpha_0 = \frac{cot\tilde{\alpha}}{2} - \frac{1}{sin(2\tilde{\alpha})}\frac{\sqrt{C_4^2 + S_4^2} - \tilde{C}_0}{\sqrt{C_4^2 + S_4^2} - C_0} \tag{2.42}$$

$$\beta_0 = \frac{1}{4}\left(arctan\frac{S_4}{C_4} - 2\alpha_0\right) \tag{2.43}$$

The symbols with tilde being obtained from the measurement with $\alpha_0 = 45°$.

The reason why the second measurement is conducted under $\alpha_0 = 45°$, is that it minimizes the errors on the calibration parameters [12]. For this calibration to work the retardance of the wave-plate must be close to 90° and α_0 close to the reference axis. The advantages of this method are that the calibration is straight-forward, as only two measurements without any realignment are necessary.

After obtaining the calibration parameters α_0, β_0 and δ the polarization can be calculated from eq. (2.29)-(2.36) This method was applied to H (horizontally linearly polarized), V (vertically linearly polarized), RC (right-circularly polarized) and E-light (eliptically polarized) to test its applicability to our setup.

3. Experimental Investigations

3.1 Experimental Equipment

3.1.1 Polarimeter

In order to measure the intensity and polarization of light the polarimeter Thorlabs PAX5710VIS-T is employed. It is able to measure the intensity and polarization of light in real-time by using the method described in section 2.6. The results of the polarization analysis, such as the azimuth, ellipticity, and DOP of a polarization ellipse, as well as the power are displayed in a GUI, where the measured polarization is represented by a point on a Poincaré-sphere, see Fig. 3.1. Instead of the ellipse parameters it can also display the Stokes parameters $\frac{M}{I}$,$\frac{C}{I}$, and $\frac{S}{I}$. An internal algorithm optimizes the calculation of the Stokes parameters for an user-specified wavelength. The reason why we can not use this device for our experiments, e.g. photoluminescence emission from a WSe_2 monolayer , is that it can not resolve the light spectrally and measures just the total intensity leading to a loss of important information.

3.1.2 Light Source

For all measurements, except the test on photoluminescence emission from a WSe_2 monolayer, the laser Coherent Lasiris SNF 660 was employed. In order to estimate whether intensity fluctuations are able to influence the following polarimetric measurements significantly, the intensity fluctuations of the laser for the duration of a full rotation of the wheel during a polarization measurement were recorded. This measurement was repeated three times. Additionally, a measurement of the intensity without a laser source only with the lab lights turned on was conducted to see if the lighting has any impact at all.

The results obtained from the noise measurement are shown in Tab. 3.1

I	σ_I	$\frac{\sigma_I}{I}$	DOP	σ_{DOP}	$\frac{\sigma_{DOP}}{DOP}$
25.564 µW	0.134 µW	0.4%	95.505	0.048	0.1%

Table 3.1: Intensity fluctuations for laser beam

With only the lab lights as an intensity source the measured intensity was in the range of 0.1 nW independent of whether they were turned on or off.

For the test on photoluminescence emission the light source was a WSe_2 monolayer, which was previously excited with a laser Sirah Matisse TR.

From the intensity measurements we see that we have intensity fluctuations of the laser in the usual range of 0.5%. This needs to be included in the error calculations, but is is not very influential in the determination of Stokes parameters.

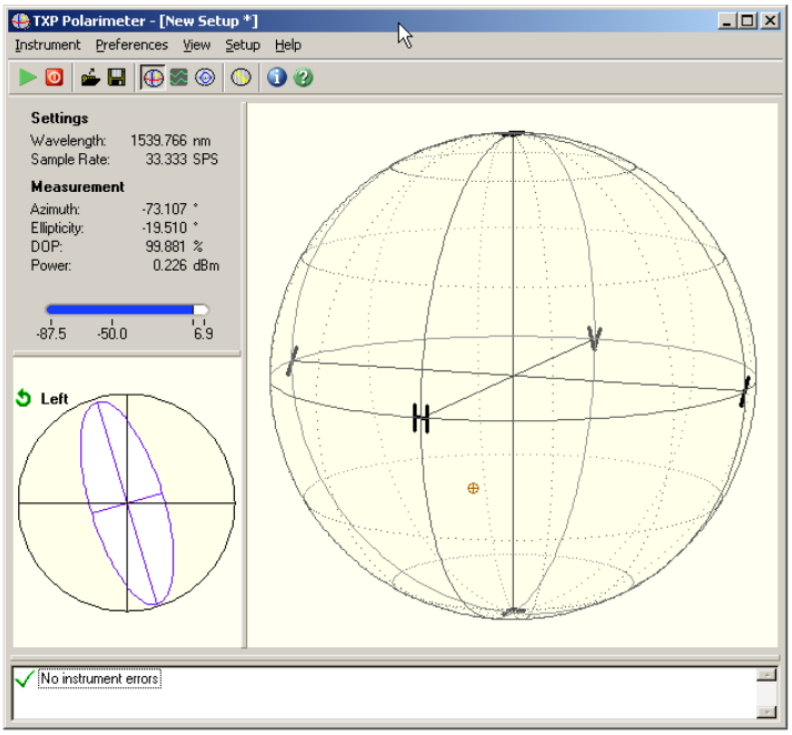

Figure 3.1: GUI for the Thorlabs polarimeter PAX5710, taken from the Thorlabs manual [13].

It is possible to cancel the effects of laser intensity fluctuations by splitting the beam with a Glan-Taylor prism before it enters the polarimetric arrangement and record its intensity fluctuations separately in a second detector. This can be used afterwards to correct the transmitted intensity from the polarimeter with the fluctuations from the laser, as it was done by Andreev[12].

The contribution from the lab lights is 5 magnitudes smaller than the recorded laser intensity. Considering that it does not change when the lights are switched on, it probably is just the internal noise of the detector. In view of that it is safe to say that the experiments can be executed with the lights turned on without any restrictions. The total indifference to lab lights is surprising, but can possibly be attributed to the design of the TXP-polarimeter, where the light has to travel a relatively long, narrow straight path inside the device before it hits the detector, effectively blocking out light that enters non-centrally or at an angle.

3.1.3 Optical Components

To make sure that the optical components we use are suitable for our subsequent measurements we analyzed their characteristics. First the intensity transmittance of the linear polarizers and retarders was examined. Three linear polarizers of the manufacturer THORlabs, 2 half-wave plates (Thorlabs SAHWP05M-1700 superachromatic 600-2700 nm and Thorlabs AHWP10M-980 achromatic 690-1200 nm) and 2 quarter-wave plates (Thorlabs AQWP10M-980 achromatic 690-1200 nm and Thorlabs SAQWP05M-1700 superachromatic 600-2700 nm) were subjected to light with pre-configured polarization. The light source was a laser Coherent Lasiris SNF 660 with an intensity of 5 mW, whose beam was led through a combination of a linear polarizer, quarter-waveplate and half-waveplate. These components were mounted to a train and could be rotated with a precision of 1°. By combining different orientations of the transmittance axes of the optical components any desired polarization of the laser beam exiting the train of optical elements could be set. We tested the components with three different polarization types (H-light, RC-light, E-light), therefore the tested

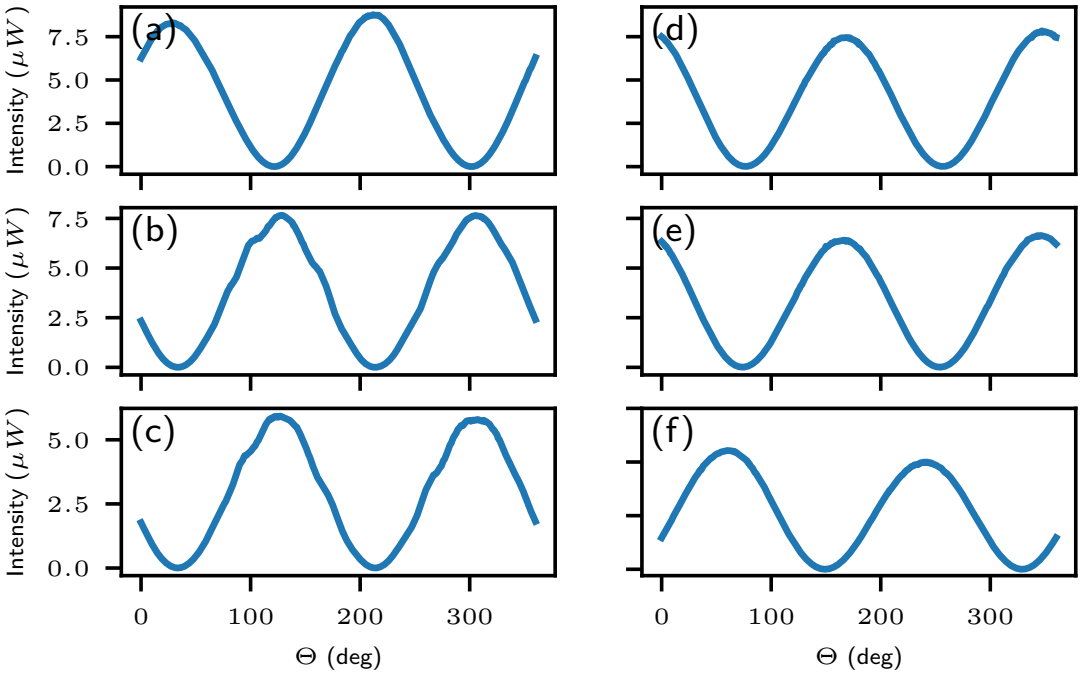

Figure 3.2: Transmitted intensity through a combination of two different linear polarizers of which the first one is at an fixed angle and the second one rotating. Combinations of different linear polarizers were tested (a) LP1/LP3, (b) LP1/LP2, (c) LP3/LP2, (d) LP3/LP1, (e) LP2/LP1, (f) LP2/LP3
. The scales in (a)-(c) are the same as in (d)-(f).

optical component was inserted into a rotating wheel (THORlabs PRM1Z8), which was connected to a DC Servo Motor Controller (Thorlabs KDC101) and rotated in steps of 1°. The transmitted intensity was recorded using the polarimeter Thorlabs PAX5710VIS-T.

Next a theoretical calculation of the transmitted intensity was done by measuring the polarization of the light coming out of the train and applying a Müller matrix of an ideal waveplate to it in order to check whether our measurements comply with our expectations.

The angular variation of the transmitted intensity for the linear polarizers was tested by rotating a LP in front of another LP and observing the intensity modulation for an incoming light beam of linearly polarized light. This was done for the three different LPs in all six possible combinations. The results can be seen in Fig. 3.2. The intensity was expected to show two minima and two maxima with the same amplitude. From these measurements the linear polarizers showing the lowest ratio between light transmitted at the minimum and the maximum were chosen under the condition that the peaks show no additional modulation after a 180° rotation to conduct a measurement of the retardance of the wave-plates.

In general all these combinations would fit for the polarization measurements. The extinction ratio r for a linear polarizer describes how much light is transmitted through its transmittance axis compared to the orthogonal axis as shown in Tab. 3.2. The error comes from laser intensity fluctuations.

The data for the linear polarizers shows that combinations involving LP1 and LP3 have the least amount of variation regarding the transmittance after a rotation by 180°, as depicted in Fig. 3.2

The combination LP1/LP3 was chosen to be the most suitable for the retardance measurement. The combination with LP2 being the second polarizer showed a bit of wobble

	r
LP1/LP3	$7.390 \pm 0.003 \times 10^{-5}$
LP1/LP2	$7.904 \pm 0.004 \times 10^{-5}$
LP3/LP2	$43.728 \pm 0.005 \times 10^{-5}$
LP3/LP1	$114.611 \pm 0.003 \times 10^{-5}$
LP2/LP1	$98.493 \pm 0.004 \times 10^{-5}$
LP2/LP3	$3.699 \pm 0.005 \times 10^{-5}$

Table 3.2: Extinction ratios r for different combinations of linear polarizers calculated from the highest minimum and lowest maximum to find an upper bound r

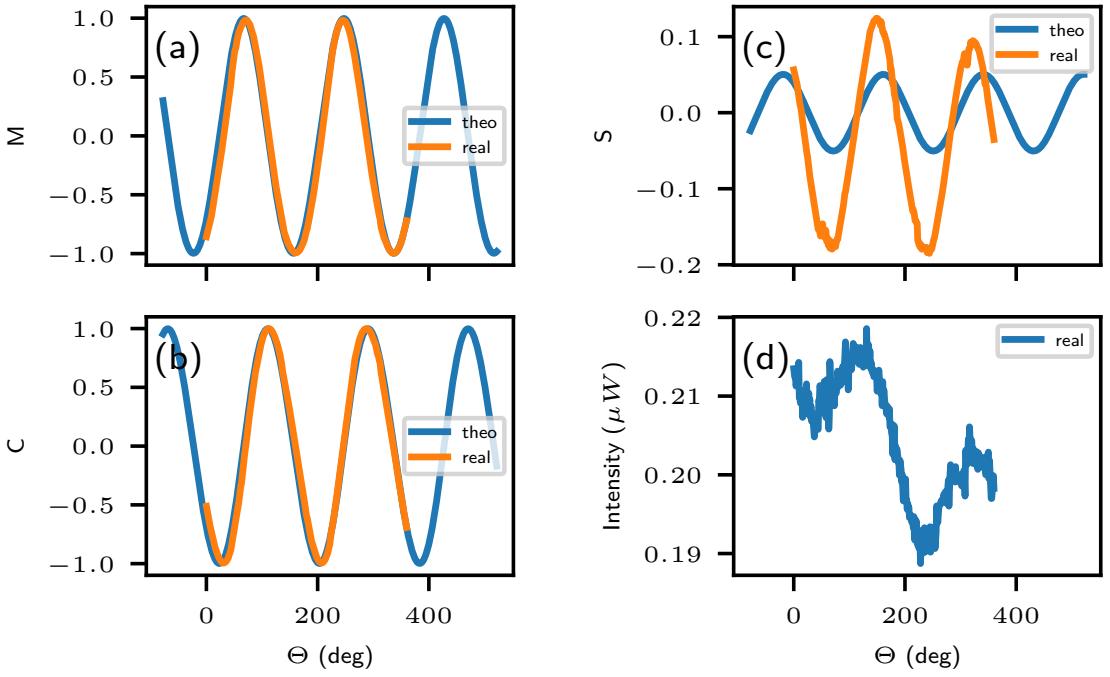

Figure 3.3: Normalized Stokes parameters (a) M, (b) C, (c) S, (d) absolute intensity for nearly ideally right-circularly polarized light (Stokes-param.: M=0.010, C=0.005, S=0.999) applied to the $\frac{\lambda}{4}$-waveplate Thorlabs SAQWP05M-1700 superachromatic 600-2700 nm)

around the maxima, which can be attributed to LP2 having non-linear attenuation. The combination of LP2/LP3 showed different amplitudes for the maxima which could possibly stem from the linear polarizers being inhomogenous meaning their transmitting and extinguishing axes are not perfectly perpendicular or from the incoming light not hitting the surface centrally.

Similarly the waveplates were rotated in the mount while being illuminated with H-, RC or E-light and the resulting intensity was compared to the theoretical calculations.

All the waveplates showed the desired behaviour, except for some angular modulation not predicted by Müller calculus with ideal optical elements, as can be seen in Fig. 3.3, Fig. 3.4, Fig. 3.5 and Fig. 3.6.

For the most part the recorded M, C and S-values corresponded to the theoretical calculations, except for an unpredicted modulation of the intensity, where a rotation of the optical component by 180° changed the transmitted intensity noticeably. This modulation could be observed in the Stokes parameters as well as the intensity and amounted to 5-10 % of the expected amplitude peaks.

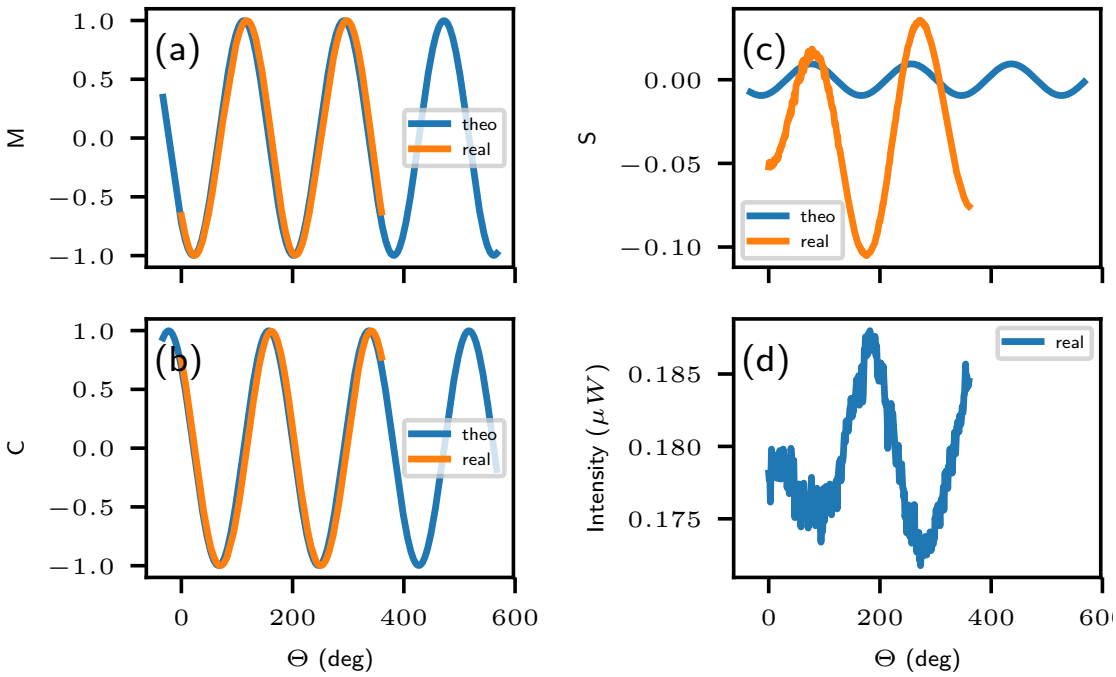

Figure 3.4: Normalized Stokes parameters (a) M, (b) C, (c) S, (d) absolute intensity for nearly ideally right-circularly polarized light (Stokes-param.: M=0.010, C=0.005, S=0.999) applied to the $\frac{\lambda}{4}$-waveplate Thorlabs AQWP10M-980 achromatic 690-1200 nm)

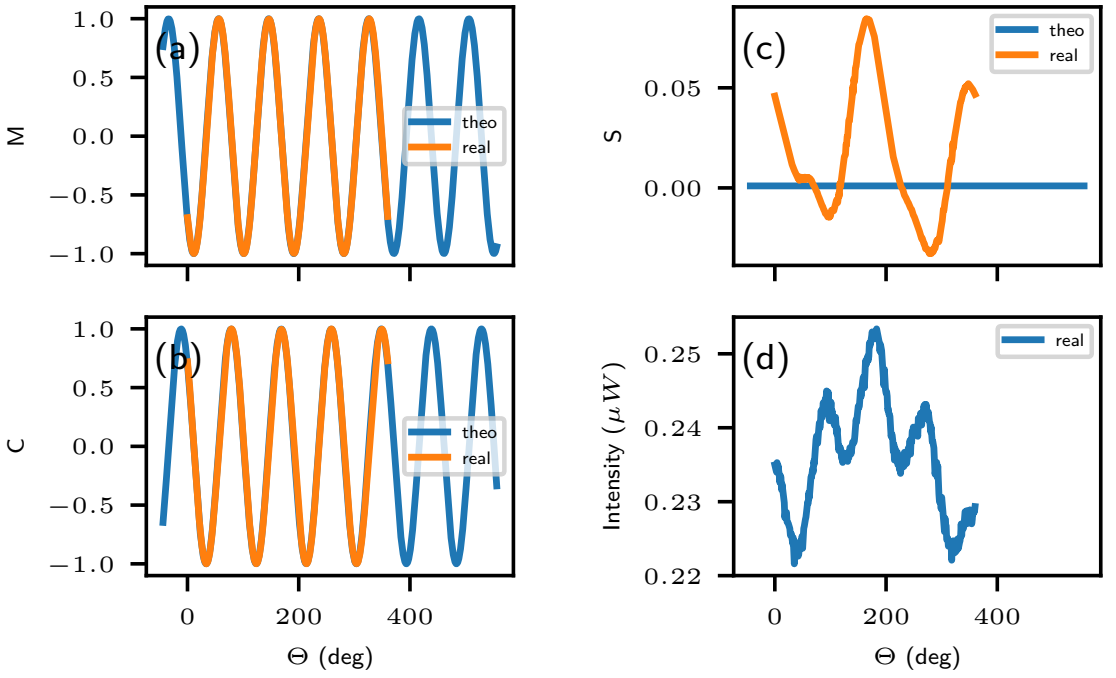

Figure 3.5: Normalized Stokes parameters (a) M, (b) C, (c) S, (d) absolute intensity for nearly ideally horizontally polarized light (Stokes-param.: M=1.000, C=0.006, S=-0.001) applied to the $\frac{\lambda}{2}$-waveplate Thorlabs SAHWP05M-1700 superachromatic 600-2700 nm

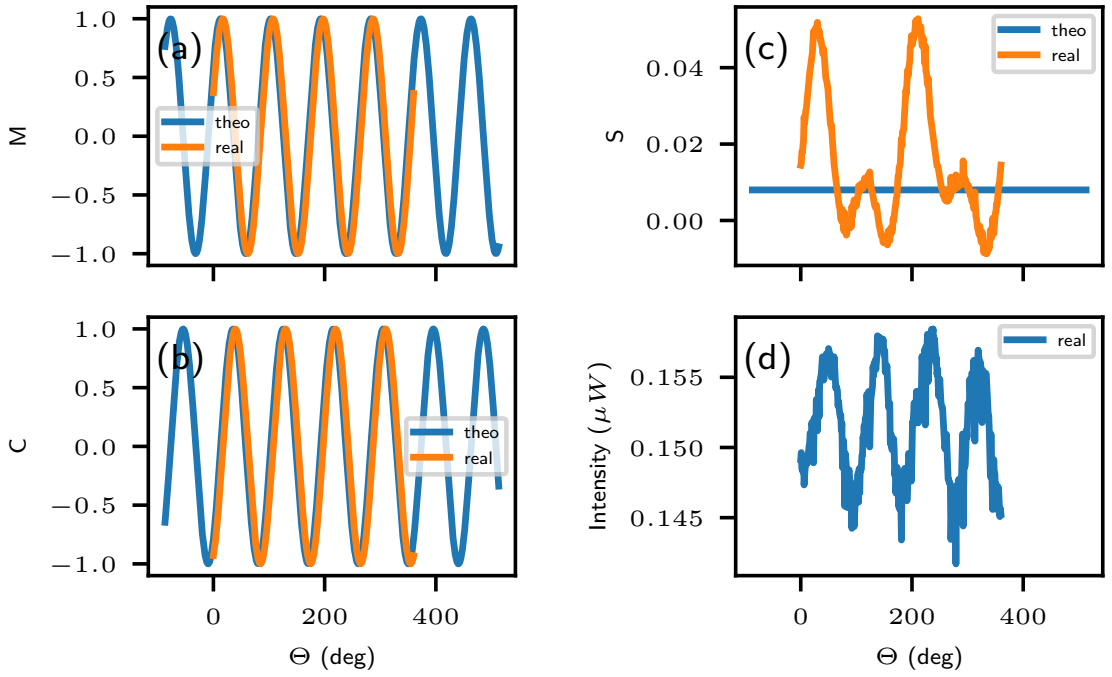

Figure 3.6: Normalized Stokes parameters (a) M, (b) C, (c) S, (d) absolute intensity for nearly ideally horizontally polarized light (Stokes-param.: M=1.000, C=0.006, S=-0.001) applied to the $\frac{\lambda}{2}$-waveplate Thorlabs AHWP10M-980 achromatic 690-1200 nm

When right-circular light is applied to a $\frac{\lambda}{4}$-waveplate the Stokes vector is projected in a Poincarè-sphere picture from the north of the sphere to various points on the equator of the sphere depending on the angle. In Fig. 3.3 (a) and (b) we see exactly this. As the Stokes vector lies on the equator after the projection, there is no circular polarization left, which can be seen in Fig. 3.3 (c). The total intensity shows a modulation around 10% of the maximum amplitude, which can be attributed to a Fabry-Pérot-type effect [14]. When horizontally-polarized light is applied to a $\frac{\lambda}{2}$-waveplate the Stokes vector is projected onto various points on the equator, but with doubled frequency, as the retardance is two times larger than for the case of a $\frac{\lambda}{4}$-waveplate, which can be seen in 3.5 (a) and (b). In (c) of Fig. 3.5 we see a similar intensity modulation as for the $\frac{\lambda}{4}$-waveplate.

3.2 Measuring retardance of waveplates by fitting Müller-matrices

In order to be able to conduct a precise polarimetric measurement we need to determine the retardance of the waveplates. One possibility to obtain the retardance is to let the waveplates rotate in the mount and then fit the respective Müller-matrices A by using the formula

$$\begin{bmatrix} I' \\ M' \\ C' \\ S' \end{bmatrix} = A \begin{bmatrix} I \\ M \\ C \\ S \end{bmatrix} \tag{3.1}$$

The Müller matrix is dependent on the orientation of the fast axis of the retarder. We took that into account by multiplying it with the rotation matrices

$$A = R^T(\beta + \beta_0) A_0 R(\beta + \beta_0) \tag{3.2}$$

and introducing an additional parameter β_0, which takes into consideration the unknown main axis of the retarder. With that we can fit all 17 parameters included in the 4x4 Müller

matrix, which is a function of the angle β by looking at the initial intensity of the laser and the transmitted intensity.

We recorded data for one full rotation, which equals to 360 data points and fitted the respective Müller matrix for each row of eq. (3.1). Accordingly, we used a total of 1440 datapoints to fit 16 entries of each matrix with 17 parameters in total. In order to avoid errors coming from fluctuating laser intensity we normalize all data points with their respective intensity. The polarimeter used for measuring the Stokes vectors considers partially polarized light by displaying the DOP

$$DOP = \frac{\sqrt{M^2 + C^2 + S^2}}{I} \tag{3.3}$$

Since our theoretical model acts on the polarized beam of the light we additionally normalize our intensities with the DOP. We approached fitting the matrices in two different ways.

In the first approach, which we call 16-parameter approach, we take all 16 values of the matrix as parameters into the curvefit function from the python scipy module and for the half-wave plate introduce boundaries for the diagonal elements between [-1,1] and for the off-diagonal elements between [-0.1, 0.1].

$$\begin{bmatrix} a_{11} & a_{12} & a_{13} & a_{14} \\ a_{21} & a_{22} & a_{23} & a_{24} \\ a_{31} & a_{32} & a_{33} & a_{34} \\ a_{41} & a_{42} & a_{43} & a_{44} \end{bmatrix}$$

Within this approach we chose the matrix for the quarter-wave plate, where all non-zero values are bounded between [-1,1] with $D = Msin\frac{1}{2}\delta$ and $G = cos\frac{1}{2}\delta$, as these are the relevant values for a waveplate in general fitting six entries of the matrix.

$$\begin{bmatrix} 1 & 0 & 0 & 0 \\ 0 & D^2 + G^2 & 0 & 0 \\ 0 & 0 & -D^2 + G^2 & 2DG \\ 0 & 0 & -2DG & 2G^2 - 1 \end{bmatrix}$$

The following matrices were obtained from fitting all sixteen parameters for the half-waveplates

Müller-matrix for half-waveplate 600-2700 nm

$$\begin{pmatrix} 0.999 & 0.000 & 0.000 & 0.002 \\ -0.004 & 1.000 & 0.100 & -0.003 \\ -0.015 & 0.075 & -1.000 & -0.007 \\ -0.100 & -0.011 & 0.032 & -0.816 \end{pmatrix}$$

Müller-matrix for half-waveplate 690-1200 nm

$$\begin{pmatrix} 1.000 & 0.000 & 0.000 & -0.002 \\ 0.001 & 0.965 & -0.100 & 0.008 \\ -0.003 & -0.098 & -1.000 & 0.003 \\ 0.100 & 0.005 & -0.007 & -0.876 \end{pmatrix}$$

The results for the half-waveplates are shown in Fig. 3.7 and Fig. 3.8.

The following matrices were obtained from fitting six parameters for the quarter-waveplates

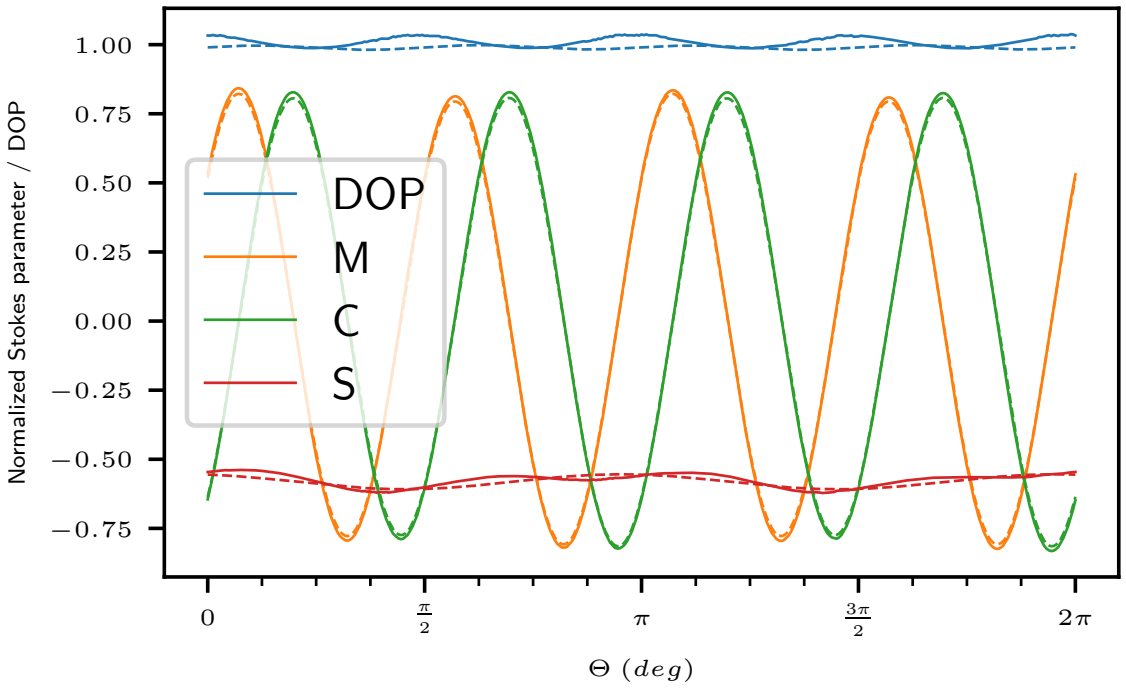

Figure 3.7: Solid curves show the normalized Stokes parameters for the $\frac{\lambda}{2}$-waveplate 600-2700 nm, dashed curves show the resulting Stokes parameters after application of the Müller-matrix fitted with the 16-parameter approach to the Stokes vector of the incoming elliptically polarized light beam (Stokes-param.: M=-0.489, C=0.637, S=0.594)

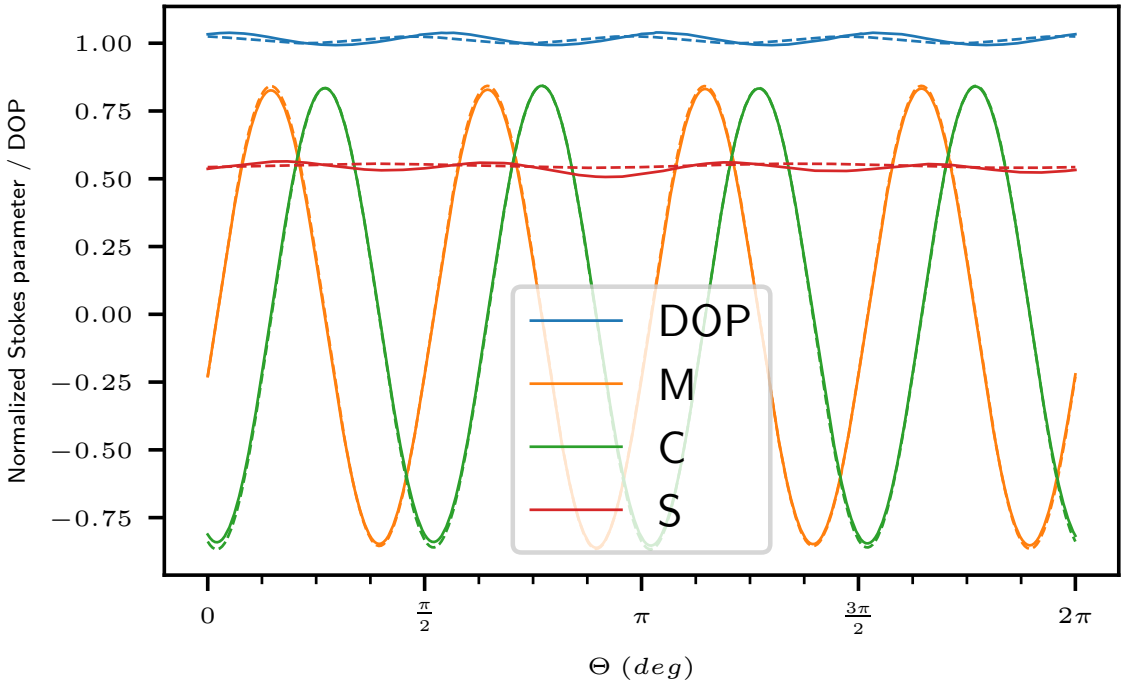

Figure 3.8: Solid curves show the normalized Stokes parameters for the $\frac{\lambda}{2}$-waveplate 690-1200 nm, dashed curves show the resulting Stokes parameters after application of the Müller-matrix fitted with the 16-parameter approach to the Stokes vector of the incoming elliptically polarized light beam (Stokes-param.: M=0.447, C=0.734, S=-0.510)

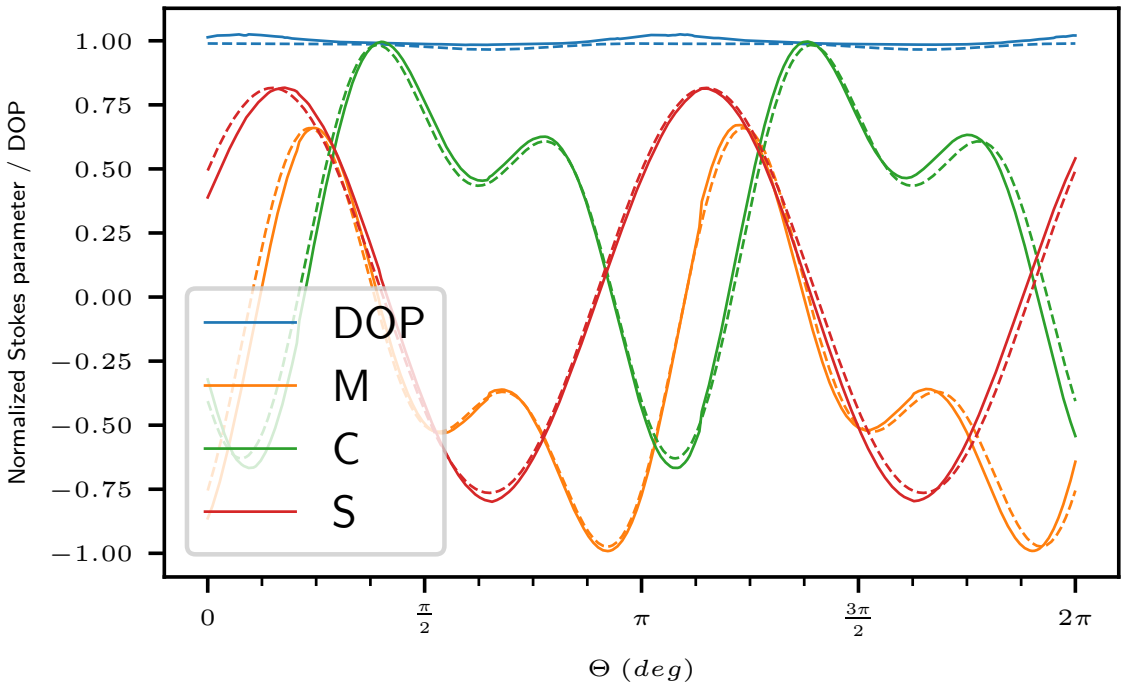

Figure 3.9: Solid curves show the normalized Stokes parameters for the $\frac{\lambda}{4}$-waveplate 600-2700 nm, dashed curves show the resulting Stokes parameters after application of the Müller-matrix fitted with the 16-parameter approach to the Stokes vector of the incoming elliptically polarized light beam (Stokes-param.: M=-0.534, C=0.616, S=0.577)

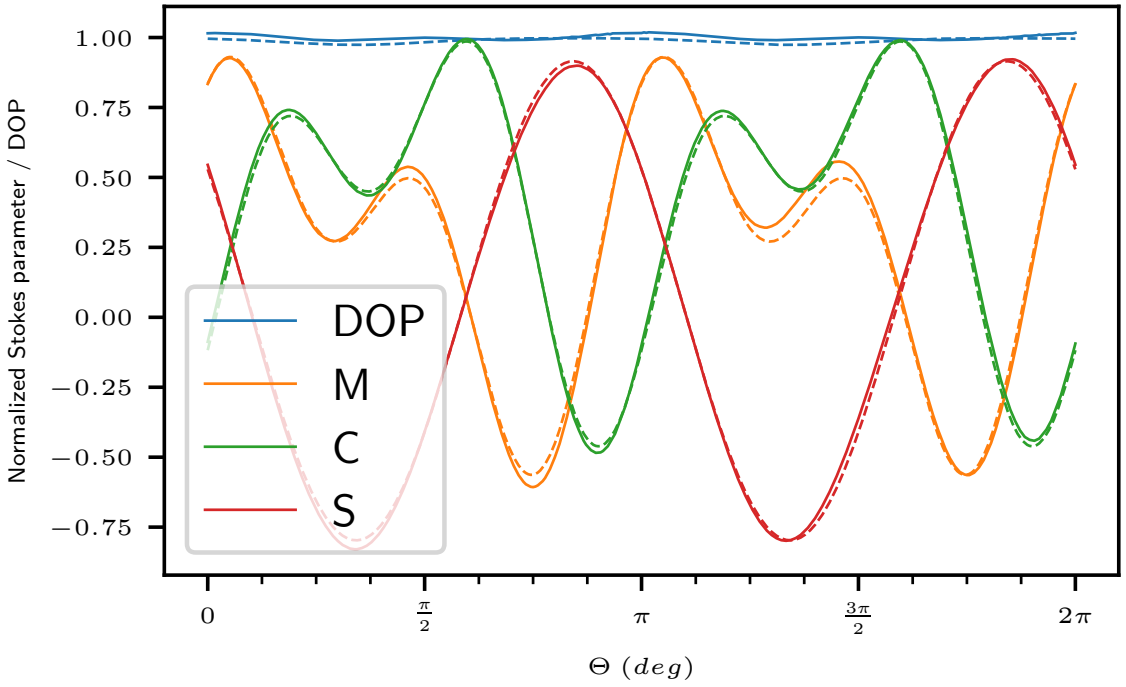

Figure 3.10: Solid curves show the normalized Stokes parameters for the $\frac{\lambda}{4}$-waveplate 690-1200 nm, dashed curves show the resulting Stokes parameters after application of the Müller-matrix fitted with the 16-parameter approach to the Stokes vector of the incoming elliptically polarized light beam (Stokes-param.: M=0.481, C=0.718, S=0.502)

Müller-matrix for quarter-waveplate 600-2700 nm

$$\begin{pmatrix} 1.000 & 0.000 & 0.000 & 0.000 \\ 0.000 & 0.990 & 0.000 & 0.000 \\ 0.000 & 0.000 & 0.021 & 1.000 \\ 0.000 & 0.000 & -0.976 & 0.045 \end{pmatrix}$$

Müller Matrix for quarter-waveplate 690-1200 nm

$$\begin{pmatrix} 1.000 & 0.000 & 0.000 & 0.000 \\ 0.000 & 1.000 & 0.000 & 0.000 \\ 0.000 & 0.000 & 0.094 & 0.950 \\ 0.000 & 0.000 & -0.989 & 0.117 \end{pmatrix}$$

The other approach we use, which we call 4-parameter approach, is fitting only the parameters, which are non-zero in the ideal Müller matrices for a half-wave plate

$$\begin{bmatrix} a_{11} & 0 & 0 & 0 \\ 0 & a_{22} & 0 & 0 \\ 0 & 0 & a_{33} & 0 \\ 0 & 0 & 0 & a_{44} \end{bmatrix}$$

and for a quarter-waveplate

$$\begin{bmatrix} a_{11} & 0 & 0 & 0 \\ 0 & a_{22} & 0 & 0 \\ 0 & 0 & 0 & a_{34} \\ 0 & 0 & a_{43} & 0 \end{bmatrix}$$

and bound them between [-1,1]. The results are shown in Fig. 3.11 and Fig. 3.12 for the quarter-waveplates and in Fig. 3.13 and Fig. 3.14 for the half-waveplates.

Müller-matrix for half-waveplate 600-2700 nm

$$\begin{pmatrix} 1.000 & 0.000 & 0.000 & 0.000 \\ 0.000 & 1.000 & 0.000 & 0.000 \\ 0.000 & 0.000 & -1.000 & 0.000 \\ 0.000 & 0.000 & 0.000 & -0.986 \end{pmatrix}$$

Müller-matrix for half-waveplate 690-1200 nm

$$\begin{pmatrix} 1.000 & 0.000 & 0.000 & 0.000 \\ 0.000 & 0.970 & 0.000 & 0.000 \\ 0.000 & 0.000 & -1.000 & 0.000 \\ 0.000 & 0.000 & 0.000 & -1.000 \end{pmatrix}$$

Müller-matrix for quarter-waveplate 600-2700 nm

$$\begin{pmatrix} 1.000 & 0.000 & 0.000 & 0.000 \\ 0.000 & 0.991 & 0.000 & 0.000 \\ 0.000 & 0.000 & 0.000 & -1.000 \\ 0.000 & 0.000 & 0.976 & 0.000 \end{pmatrix}$$

Müller Matrix for quarter-waveplate 690-1200 nm

$$\begin{pmatrix} 1.000 & 0.000 & 0.000 & 0.000 \\ 0.000 & 1.000 & 0.000 & 0.000 \\ 0.000 & 0.000 & 0.000 & -0.950 \\ 0.000 & 0.000 & 0.989 & 0.000 \end{pmatrix}$$

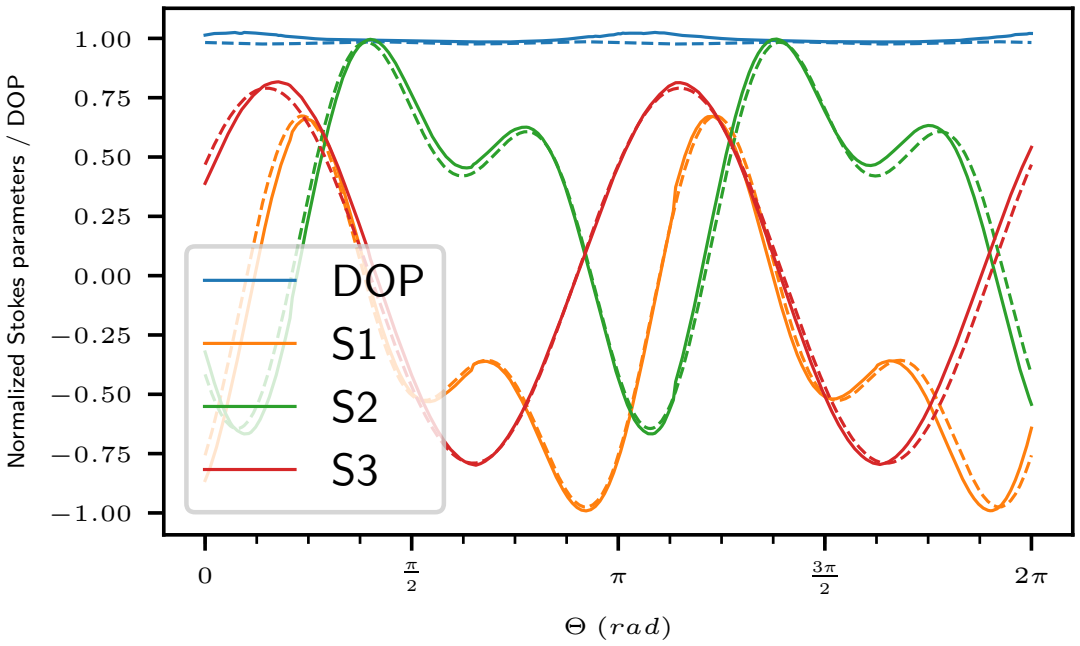

Figure 3.11: Solid curves show the normalized Stokes parameters for the $\frac{\lambda}{4}$-waveplate 600-2700 nm, dashed curves show the resulting Stokes parameters after application of the Müller-matrix fitted with the 4-parameter approach to the Stokes vector of the incoming elliptically polarized light beam (Stokes-param.: M=-0.534, C=0.616, S=0.577)

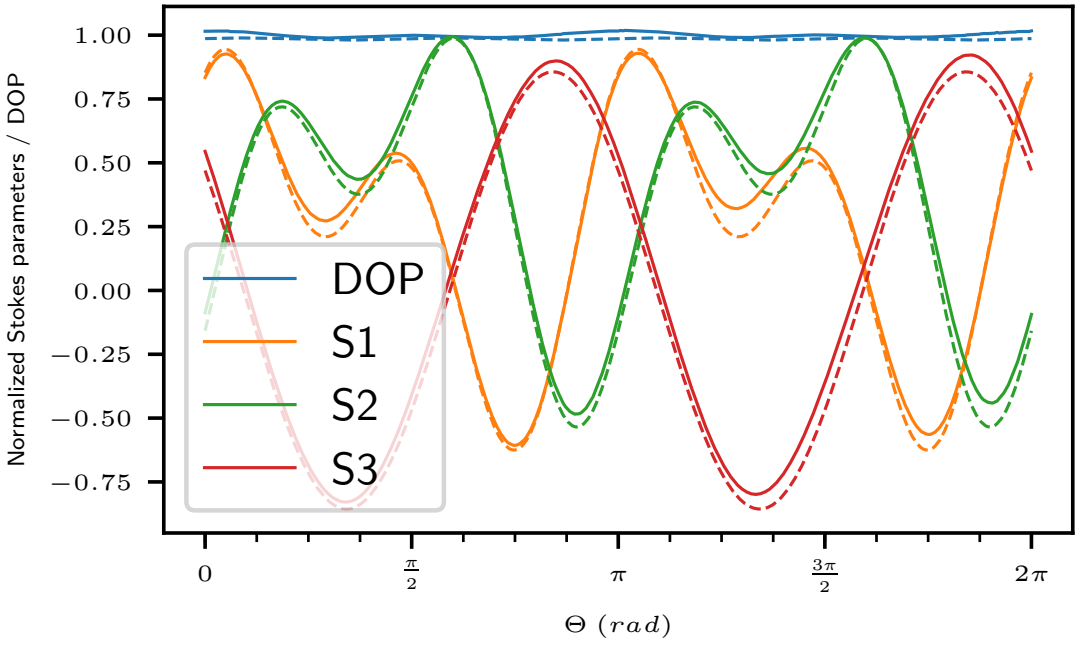

Figure 3.12: Solid curves show the normalized Stokes parameters for the $\frac{\lambda}{4}$-waveplate 690-1200 nm, dashed curves show the resulting Stokes parameters after application of the Müller-matrix fitted with the 4-parameter approach to the Stokes vector of the incoming elliptically polarized light beam (Stokes-param.: M=0.481, C=0.718, S=0.502)

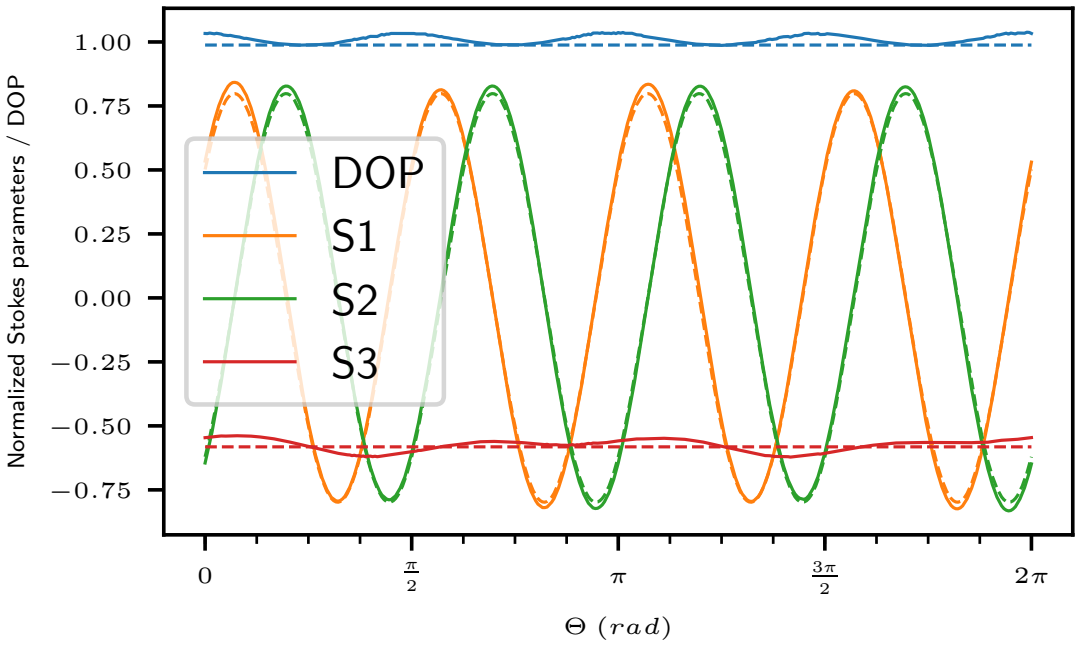

Figure 3.13: Solid curves show the normalized Stokes parameters for the $\frac{\lambda}{2}$-waveplate 600-2700 nm, dashed curves show the resulting Stokes parameters after application of the Müller-matrix fitted with the 4-parameter approach to the Stokes vector of the incoming light beam

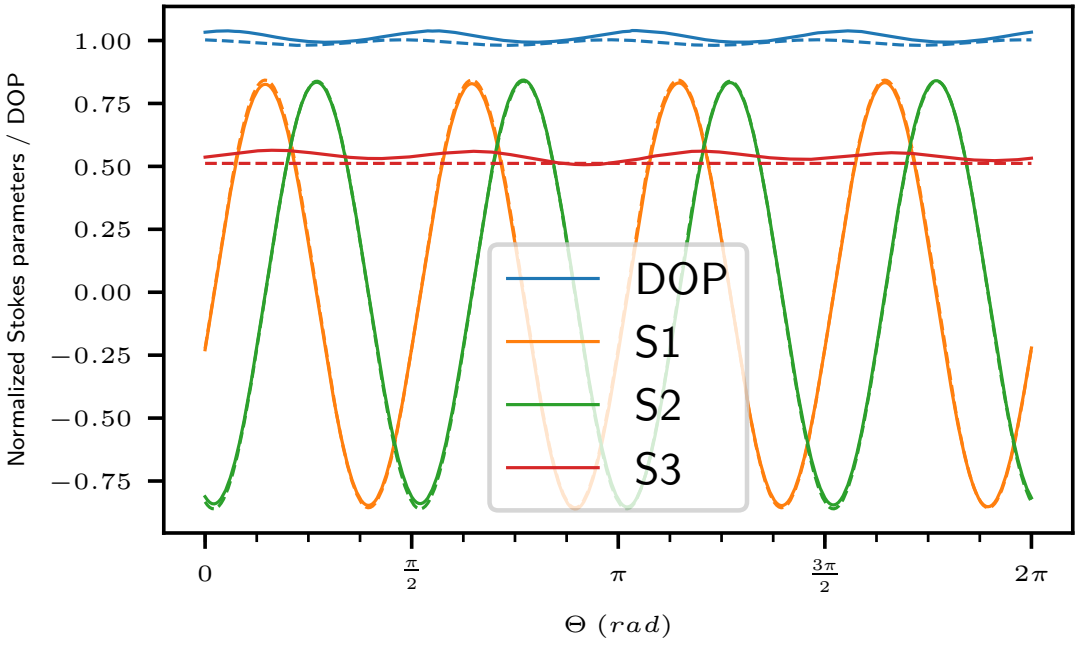

Figure 3.14: Solid curves show the normalized Stokes parameters for the $\frac{\lambda}{2}$-waveplate 690-1200 nm, dashed curves show the resulting Stokes parameters after application of the Müller-matrix fitted with the 4-parameter approach to the Stokes vector of the incoming light beam

The Müller-matrices for the waveplates have in common that many of the fitted values are close to our bounds of [-1,1] and if we loosen the restrictions the optimal values for our matrix entries usually exceed |1|. Physically for an ideal waveplate entries higher than |1| are not possible, as this would correspond to creation of intensity within the waveplate. This tells us that our model of ideal waveplates has flaws, e.g. it does not consider interference effects within the waveplate, which lead to an additional angular modulation of the intensity. We can determine the retardance of the waveplates from observing the difference between incoming and outgoing Stokes-vector, e.g. a change from horizontal to anti-horizontal polarization would correspond to a retardance of 180°. After applying the fitted matrices to theoretically ideally linearly polarized light, we can extract the retardance by

$$\delta = (\Delta D - \Delta H) \cdot \frac{180}{2} \tag{3.4}$$

where

$$\Delta H = M - M^{'} \tag{3.5}$$

$$\Delta D = C - C^{'} \tag{3.6}$$

with the prime indicating Stokes parameters of the outgoing light. The results for the retardances determined from fitting Müller-matrices are shown in Tab. 3.3.

	$\delta_{\frac{\lambda}{2}-WP\ 600-2700\ \mathrm{nm}}$	$\delta_{\frac{\lambda}{2}-WP\ 690-1200\ \mathrm{nm}}$	$\delta_{\frac{\lambda}{4}-WP\ 600-2700\ \mathrm{nm}}$	$\delta_{\frac{\lambda}{4}-WP\ 690-1200\ \mathrm{nm}}$
16-param. approach	180.98°	178.29°	87.28°	88.11°
4-param. approach	180.00°	177.29°	89.18°	90.00°

Table 3.3: Results calculating retardances from applying fitted matrices to ideal Stokes vectors

3.3 Determining retardance of quarter-waveplate with method of rotating plates

The aim of this section is to determine the retardance of a quarter-waveplate by the method of rotating plates. To account for non-ideal linear polarizers we need to determine the efficiency k_{inc} of the combination of linear polarizers P1 and P2 show in eq.(3.7), where I_{max} is the transmitted intensity when their axes are parallel and I_{min} when crossed.

$$\frac{M}{I} = k_{inc} = \frac{I_{max} - I_{min}}{I_{max} + I_{min}} \tag{3.7}$$

The retardance was then measured by putting the transmission axis of P1 (LP between laser and rotating wheel) parallel to the x-axis and the axis of P2 (LP between rotating wheel and polarimeter) at $\alpha = \frac{\pi}{4}$ and doing a full rotation for each of the quarter-waveplates with

$$\delta = arccos\left[\frac{1 - |\eta| cos2\alpha - 2\frac{|\eta|}{k_{inc}}}{1 + |\eta| cos2\alpha}\right] \tag{3.8}$$

The modulation ratio $|\eta|$ needs to be determined from the transmitted intensity.

$$\eta = \frac{I_{max} - I_{min}}{I_{max} + I_{min}} = \frac{M(1 - cos\delta)}{2I + Mcos2\alpha(1 + cos\delta)} \tag{3.9}$$

This measurement was repeated ten times for each of the $\frac{\lambda}{4}$-waveplates.

We plugged the measured variables into eq. (3.8).

The efficiency of the combination of linear polarizers P1 and P3 was calculated. From the ten measurements the mean and the standard deviation of the efficiency was obtained, as seen in Tab. 3.4. There is also an error originating in the modulation of intensity due to waveplate ripple, shown in Fig. 3.15 and Fig. 3.16.

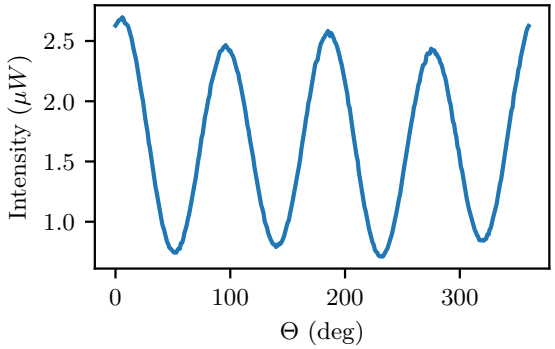

Figure 3.15: Transmitted intensity for rotating QWP 690-1200 nm between two LPs

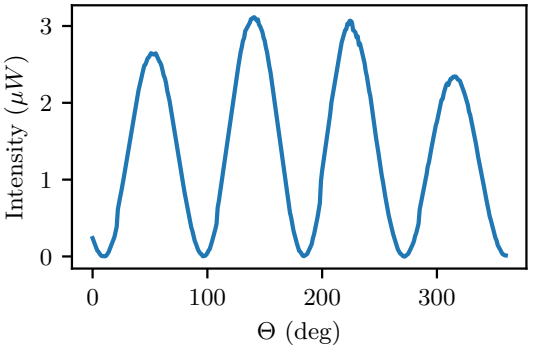

Figure 3.16: Transmitted intensity for rotating QWP 600-2700 nm between two LPs

We estimate the error $\sigma_{I_{max},rip.}$ from waveplate error for I_{max} to be 40% of the difference between the highest and the lowest maximum, as for a regular non-achromatic waveplate the peaks would have approximately the same amplitude. Accordingly, the same error estimation $\sigma_{I_{min},rip.}$ was done for I_{min} resulting in an error of the retardance $\sigma_{\bar{\delta},rip.}$

	k_{inc}	$\sigma_{k_{inc}}$	$\bar{\delta}$ (deg)	$\sigma_{\bar{\delta},stat}$(deg)	$\sigma_{I_{max},rip.}$(µW)	$\sigma_{I_{min},rip.}$(µW)	$\sigma_{\bar{\delta},rip.}$(deg)	$\bar{\delta}_{adj.}$(deg)	$\sigma_{\bar{\delta}_{adj.}}$
QWP 690-1200 nm	0.999	$2 \cdot 10^{-7}$	99.46	0.35	0.09	0.05	85.24	93.76	0.33
QWP 600-2700 nm	0.999	$2 \cdot 10^{-7}$	105.09	0.40	0.34	0.11	83.71		

Table 3.4: Retardances of the quarter-waveplates obtained by the method of rotating plates

The statistical errors are small, as they depend mainly on the laser intensity fluctuations. The errors from the waveplate ripple $\sigma_{\bar{\delta},rip.}$ are very large in the order of the value for the retardance, which leads us to the conclusion that the effects of an achromatic waveplate are not taken into account by this method and thus it is not suitable for the determination of the retardance.

Another method would be to determine the retardance from each adjacent minimum and maximum, take the mean of the 4 resulting values and then average the resulting values for the 10 measurements to obtain $\sigma_{\bar{\delta}_{adj.}}$.

This method for determining the retardance is supposed to be robust, as there is only one simple calibration for the efficiency of the linear polarizer needed beforehand and there are no diverging parts in the formula for determining $\delta(\lambda)$. Nonetheless, the retardance for the quarter-waveplate 690-1200 nm deviates around 10% and the one for quarter-waveplate 600-2700 nm even more with around 15% from the expected retardance of 90°. If that

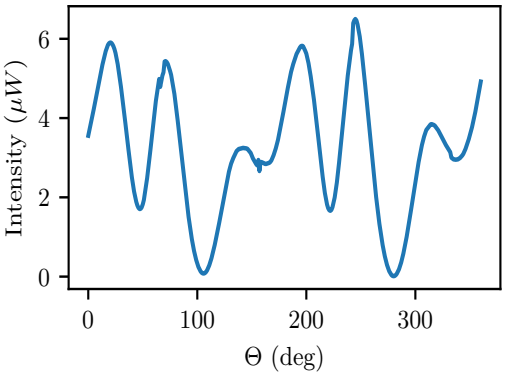

Figure 3.17: Transmitted intensity for determining retardance of QWP $\frac{\lambda}{4}$-waveplate when tilted left by 20°

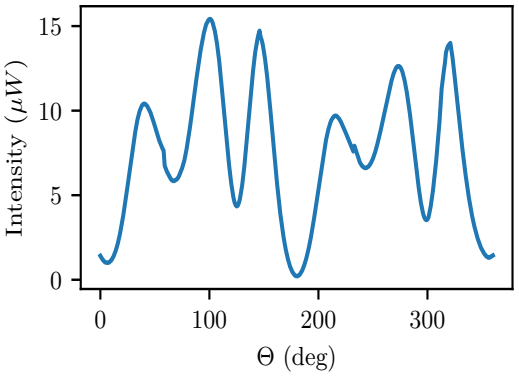

Figure 3.18: Transmitted intensity for determining retardance of QWP $\frac{\lambda}{4}$-waveplate when tilted right by 20°

was true our waveplates would be unusable for our polarimeter, as such a heavy error would introduce very large errors to our Stokes parameters. We argue that this method is not suitable for finding the retardance of the waveplates, as it ignores the modulation in the amplitude, coming from a Fabry-Pérot-type effect typical for achromatic waveplates. Considering that $\cos(\delta)$ depends linearly on $\eta = \frac{I_{max}-I_{min}}{I_{max}+I_{min}}$ any change in the extrema of the intensity disturbs the ratio and correspondingly $\cos(\delta)$. If we assume an error of 5-10% of the amplitudes of the peaks from the mean of the peaks we get a large error on the retardance from gaussian error propagation.

We checked whether the retardance of the quarter-waveplate is influenced by the rotation of the retarder out of the plane standing perpendicular to the propagation direction of the light. Therefore, we executed two measurements of the retardance with the method described in the previous section, where we tilted the quarter-waveplate around 20° about its vertical axis. The measurement was repeated for each direction of rotation 10 times. The transmitted intensity can be seen in Fig. 3.17 and Fig. 3.18. The results are shown in Tab. 3.5.

	$k_{inc}(\lambda)$	$\sigma_{k_{inc}(\lambda)}$	$\bar{\delta}$	$\sigma_{\bar{\delta}}$
QWP 600-2700 nm tilt left	0.999	$2 \cdot 10^{-}7$	174.08	0.87
QWP 600-2700 nm tilt right	0.999	$2 \cdot 10^{-}7$	159.96	1.52

Table 3.5: Retardances of the quarter-waveplates tilted by 20° obtained by the method of rotating plates

The results indicate that the tilt of the quarter-waveplates face-side has a substantial effect on the retardance, as it nearly changes the plates to half-wave plates. We can also exclude the possibility of having the quarterwave-plates switched with half-waveplates by mistake and measuring them instead, as the transmitted intensity behaves uniquely displaying 6 modulated peaks in contrast to the expected two peaks for a half-wave plate. We did not measure the change of the retardance over the course of multiple tilt angles, as we did not have precise instruments at hand to measure the rotation of the wheel. Anyways, it is not hard to do with the right equipment and would be useful in order to estimate the importance of a precise calibration. However, from our results for a tilt of 20° we can guess, that already small misalignments around a few degrees change the retardance drastically.

Another method to determine the retardance of the quarter-waveplate 600-2700 nm is described in section 2.7. The experimental implementation of this method is described in a later section, but the results are shown here in order to compare all three methods for

determining the retardance thereafter.

$$\delta = 86.89 \pm 0.23^\circ$$

3.4 Comparison determining the retardance from three different methods

After having determined the retardance with three different methods we compared the results shown in Tab. 3.6 in order to determine the most precise one. The method described in section 3.3 where the rotating retarder was placed between two linear polarizers is the simplest and for a monochromatic retarder the preferred method. Unfortunately, in our case with the achromatic retarder an additional angular modulation due to waveplate ripple exists, which changes the maximum and minimum intensities used to determine the retardance.

The determination of the retardance from fitting the Müller-matrices suffers from the same problem, as the entries of the Müller-matrices would have to be weighted according to the non-ideal behaviour of the quarterwave-plate. Applying the fitted matrices to the incoming laser beam leads to theoretical predictions of the transmitted intensity close to the measured one, but that does not mean necessarily that the calculated Müller matrices for the quarterwave-plate correspond to its real characteristics. The scope of Müller matrices fulfilling the requirements of the fit was wide and they were heavily influenced by the choice of arbitrary boundary conditions.

The best method is calculating the retardance from the Fourier coefficients within the approach of the self-calibrating polarimetric method from section 2.7 involving a linear polarizer and a retarder, as they are not influenced by the waveplate ripple.

Method	$\delta_{QWP600-2700\text{nm}}$	$\delta_{QWP690-1200\text{nm}}$
Rotating plates	$105.09 \pm 0.40^\circ$	$99.46 \pm 0.35^\circ$
Fitting Müller-matrices(16-param.)	87.28°	88.11°
Fitting Müller-matrices(4-param.)	89.18°	90.00°
Self-calibrating polarimetry	$86.89 \pm 0.23^\circ$	

Table 3.6: Comparison of the results for the retardance of the $\frac{\lambda}{4}$-waveplate Thorlabs SAQWP05M-1700 superachromatic 600-2700 nm obtained by four different methods

3.5 Implementation of a motorized polarimeter with spectral resolution

3.5.1 Setup

In this section the experimental setup for a polarimeter with spectral resolution is described. To determine the Stokes parameters we used the method developed by Berry [15], which is described in section 2.6, where we set up a quarter-wave plate on a rotating mount followed by a static linear polarizer.

Two tower blocks with openings were installed through which a laser beam could be guided. At the opening of the last tower block the polarimeter Thorlabs PAX5710VIS-T was installed. Between the top of the two tower blocks rails were inserted, so that optical elements could be hanged from them into a laser beam path. For the rotating wheel Thorlabs PRM1Z8 - different waveplates could be inserted into its mount and it was placed on a standing foot between the tower blocks. A linear rotatable polarizer was placed in front of the polarimeter. In a QTlabs framework the rotating stage and the TXP polarimeter were programmed to do a coordinated rotation and measurement and the results were displayed in real-time.

3.5.2 Test on laser light

3.5.2.1 Polarization measurement using one retarder and a polarizer

We employ the method described in section 2.6 for determining the polarization. Therefore, we add a laser and a train of optical elements to the polarimeter setup described in section 3.5.1. We fixed the small laser Coherent Lasiris SNF 660 with λ= 660 nm and guided the laser beam using two mirrors through the openings of two tower blocks. The laser beam was calibrated with a pinhole to enter the opening of the tower blocks centrally and hit the detector of the polarimeter in the middle. The height of the rotating wheel was adjusted so that the light beam hit the waveplate centrally. Also, the plane of the waveplate was rotated to be as perpendicular to the laser beam as possible. The linear polarizer LP2, the half-waveplate 600-2700 nm and the quarter-waveplate 690-1200 nm were assembled in series to a train, which was used to control the polarization of the incoming laser beam by rotating each of the optical components to their corresponding angles. For a full rotation of the wheel we take 360 data points with $\Delta\beta = 1°$

Uncertainties arise from intensity fluctuations of the laser, finite precision in the rotation of the motorized wheel, and finite precision in setting the angles of the linear polarizer by hand.

We conducted measurements with the typical polarizations: H, RC, LC, E.

As the choice of the reference plane is arbitrary, we chose $\alpha = 0$ to be the angle, where the TXP polarimeter measures the highest horizontal polarization after sending laser light through a linear polarizer. We calculate the initial retarder angle according to formula

$$\beta_0 = \frac{arctan(\frac{S_4}{C_4}) - 2\alpha}{4} \tag{3.10}$$

where the coefficients are taken from a measurement for horizontally polarized light.

Because the result from arctan $\left(\frac{x}{y}\right) \in \left[\frac{\pi}{2}\ \frac{\pi}{2}\right]$ can be ambigious we use the arctan2(x,y) function from the numpy package to map our angle to the right quadrant in the unit circle, as shown in Tab. 3.7, yielding $\beta_0 = 29.84° \pm 1.02°$.

x	y	$arctan2(\frac{x}{y})$
$\pm$ 0	0	$\pm$ 0
$\pm$ 0	-0	$\pm\ \pi$
> 0	$\pm$ inf	$0/\ \pi$
<0 0	$\pm$ inf	$0/\ -\pi$
$\pm$ inf	+ inf	$\pm\ \frac{\pi}{4}$
$\pm$ inf	- inf	$\pm\ \frac{3\pi}{4}$

Table 3.7: Values for arctan2 function

The retardance for the quarter-waveplate determined with the 16-parameter approach was used for the calculations, as this method has the least arbitrary restrictions, like fitting only values that suit our model and the choice of restrictions influences the outcome for the retardance heavily. Accordingly its usage in the subsequent calculations needs to be handled carefully.

$$\delta_{\frac{\lambda}{4}-WP\ 600-2700\ \text{nm}} = 87.28°$$

There is a discrepancy between the choice of this method and the conclusions presented in section 3.4 for the best method for determining the retardance, which is the self-calibrating

polarimetric method, but at the moment of the polarization measurement using one retarder and a polarizer the self-calibrating method was unknown to the experimenter.

The error was estimated to 1° from comparing with the results from the matrix fits, where more entries within the matrix were strictly bounded. The error on the angle α_0 was estimated to 1° from manually aligning the transmittance axis of the linear polarizer. The error on the intensity was already determined in section 3.1.1.

With the method described in section 2.6 we obtain following results as shown in Tab. 3.8 for measurements with different polarizations.

	$\frac{M}{I}$	$\frac{C}{I}$	$\frac{S_{fromS_2}}{I}$	$\frac{S_{fromC_2}}{I}$	$\frac{\lvert S\rvert}{I}$	$\frac{\lvert M\rvert}{I}$	$\frac{L}{I}$
H-light	0.953 ± 0.077	0.000 ± 0.042	-0.117 ± 0.006	0.074 ± 0.004	0.104 ± 0.005	0.869 ± 0.081	0.953 ± 0.045
H-light exp	1.000	-0.004			0.003		1.000
LC-light	0.161 ± 0.007	-0.238 ± 0.015	0.538 ± 0.013	-1.601 ± 0.023	-0.914 ± 0.006	0.548 ± 0.008	0.287 ± 0.008
LC-light exp	0.234	0.009			-0.972		0.234
RC-light	0.116 ± 0.007	0.018 ± 0.005	-0.565 ± 0.013	1.785 ± 0.025	1.004 ± 0.006	0.224 ± 0.005	0.117 ± 0.005
RC-light exp	0.097	0.114			0.988		0.149
E-light	0.597 ± 0.002	-0.673 ± 0.049	0.159 ± 0.005	-0.902 ± 0.020	-0.463 ± 0.008	1.715 ± 0.008	0.900 ± 0.023
E-light exp	0.602	0.647			-0.466		0.883

Table 3.8: Results from measurement of the Stokes parameters with method involving one retarder and one linear polarizer. The expected values come from a measurement of the polarized laser light using the polarimeter Thorlabs PAX5710VIS-T.

The calculations yielded two different values for circular polarization, as it can be calculated from the Fourier coefficients S_2 and C_2. This is due to the fact that the denominator in eq. (2.35) for S can vanish for some angles. For a more robust expression for circular polarization we need to regard the value from |C| and choose the sign from the calculation for C, which has the higher absolute value. A similar idea was used by Andreev [12].

There are some discrepancies with the expected values for horizontal and diagonal polarizations. Therefore, it is helpful to look at

$$L = \sqrt{M^2 + C^2} = \frac{\sqrt{C_4^2 + S_4^2}}{sin(\frac{\delta}{2})^2} \tag{3.11}$$

for the linear polarization, as it is more robust [12] than the expressions for horizontally and diagonally linearly polarized light and can be calculated from the Fourier coefficients.

This approach leads us to the expected values from the polarimeter measurement, where the values from $\frac{|S|}{I}$ and $\frac{|L|}{I}$ correspond well to the expectations, while the values from the other Stokes-parameters fit only well for particular polarizations, e.g are $\frac{|M|}{I}$, $\frac{S_{fromS_2}}{I}$ and $\frac{S_{fromC_2}}{I}$ only suitable with horizontally linearly polarized light,that is why some of the values for the Stokes-parameters exceed 1 clearly, which makes it very hard to judge their correctness for the usual case that the polarization of the incoming light is unknown.

The duration for the measurement of the polarization was about ten minutes for a full rotation of the wheel, as it went through all 360 angles. Therefore, we examined to which degree is it possible to reduce the number of recorded angles, while maintaining plausible results for the Stokes parameters in order to accelerate the measurements. Thus, we conducted multiple measurements with 180, 90, 45, 25, 12 or 6 equal angular steps employing the quarter-waveplate method by Berry [15] described in section 2.6. The incoming light beam was nearly ideally right-circularly polarized (M=0.110, C=0.082, S=0.990).

As the intensity is related to the Fourier coefficients

$$I_T(\beta) = C_0 + C_2 sin(2\beta) + C_4 sin(4\beta) + S_2 sin(2\beta) + S_4 sin(4\beta) \tag{3.12}$$

we can calculate the respective Fourier coefficient for each data point

$$C_0^i = I_{T_i} - C_2 cos(2\beta_i) - S_2 sin(2\beta_i) - C_4 cos(4\beta_i) - S_4 sin(4\beta_i) \tag{3.13}$$

The error is estimated according to

$$\sigma^2 = \frac{1}{N}\sum_{i=1}^{N}(C_0^i - C_0)^2 \tag{3.14}$$

The results are shown in Fig. 3.19 and Fig. 3.20. Similarly, we can calculate the errors on C_2. In the calculation for C_0 and C_2 only the first 30 angle positions were considered, otherwise small errors in the parameters are given to much weight due to cosine terms in the denominator. The results are shown in Tab. 3.9 with two entries being empty due to divergent behaviour during the calculation.

# data points	360	180	90	45	25	12	6
C_0	$6.103 \cdot 10^{-6}$	$5.434 \cdot 10^{-6}$	$6.063 \cdot 10^{-6}$	$6.130 \cdot 10^{-6}$	$5.443 \cdot 10^{-6}$	$5.382 \cdot 10^{-6}$	$5.149 \cdot 10^{-6}$
σ_{C_0}	$4.694 \cdot 10^{-7}$	$5.569 \cdot 10^{-7}$	$7.647 \cdot 10^{-7}$	$1.394 \cdot 10^{-6}$	$2.028 \cdot 10^{-6}$	$2.138 \cdot 10^{-6}$	$1.402 \cdot 10^{-6}$
$\frac{\sigma_{C_0}}{C_0}$	0.076	0.102	0.126	0.227	0.372	0.397	0.272
C_2	$3.846 \cdot 10^{-6}$	$2.567 \cdot 10^{-6}$	$4.442 \cdot 10^{-6}$	$5.146 \cdot 10^{-6}$	$4.017 \cdot 10^{-6}$	$5.908 \cdot 10^{-6}$	$3.846 \cdot 10^{-6}$
σ_{C_2}	$2.685 \cdot 10^{-6}$	$2.403 \cdot 10^{-6}$	$5.378 \cdot 10^{-6}$	$1.443 \cdot 10^{-6}$		$4.705 \cdot 10^{-6}$	$2.685 \cdot 10^{-6}$
$\frac{\sigma_{C_2}}{C_2}$	0.698	0.936	1.216	2.805		0.689	0.698

Table 3.9: Fourier coefficients C_0 and C_2 with errors for different amount of data points taken during a full rotation of the wheel

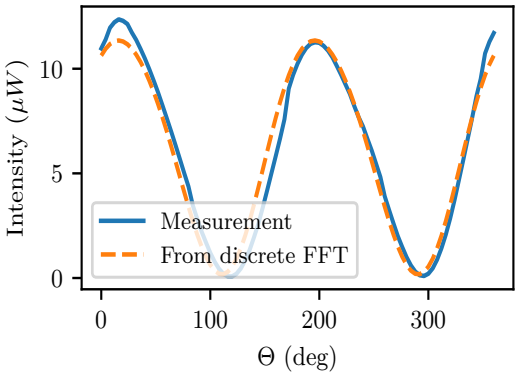

Figure 3.19: Measured intensity and calculated intensity from Fourier coefficents for achromatic $\frac{\lambda}{4}$-waveplate 600-2700 nm for 90 datapoints

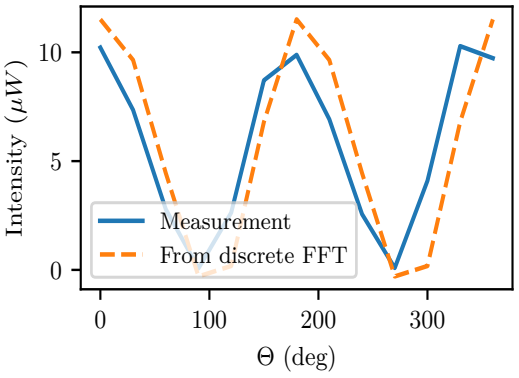

Figure 3.20: Measured intensity and calculated intensity from Fourier coefficents for achromatic $\frac{\lambda}{4}$-waveplate 600-2700 nm for 12 datapoints

Up to 90 data points the error on C_0 remains at around 10%, which is high, but the calculated intensity still fits the measurement, as seen in Fig. 3.19. Starting from 45 data points we get errors around 25% and higher, which begin to make the whole measurement questionable. Data at 12 and 6 recorded data points must be disregarded, as it fails to resemble a sine curve at all, as seen in Fig. 3.20. Similar relative errors could have been calculated for the remaining Fourier coefficients, but as sine and cosine functions figure there as the denominator, the calculations become quickly imprecise. Realistically, it is possible to reduce the time for a polarization measurement with this method to 2-3 minutes. The speed can be improved greatly by making the communication between the software and hardware more effective, as for now it does not use the full rotation speed potential of the wheel. But even without that the measurement is very practicable in a laboratory setting.

3.5.2.2 Self-calibrating polarization measurement using one retarder and a polarizer

For the determination of the polarization the self-calibrating method described in section 2.7 was employed. It was applied to H, V, RC and E-light to test its applicability to our setup.

The errors on the calibration parameters α_0, β_0, and δ stem from the intensity fluctuations of the laser, the finite precision in the rotation of the motorized wheel and from finite precision in the adjustment of the angle of the linear polarizers transmission axis. The intensity fluctuations of about 1% of the total laser power and the accuracy of the rotating wheels ability to position, estimated conservatively to about $\pm 0.3°$ [16], contribute roughly in the same order to the errors on the Fourier coefficients. The error on the retardance σ_δ consists of the errors on the Fourier coefficients C_4, S_4, and C_0 in parts of the same magnitude. The largest contribution to the error σ_{α_0} on the angle of the transmittance axis of the linear polarizer α_0 has the angle of the linear polarizer during the second measurement $\tilde{\alpha} = 45°$ with $\sigma_{\tilde{\alpha}} = \pm 1°$ from the manual setup. The contribution from the errors on the Fourier coefficients is an order of magnitude smaller. Similar relations are true for the error σ_{β_0}, where the error from the calibrated angle α_0 is more important than the errors from S_4 and C_4.

The calculation of errors on the Stokes parameters is straight-forward using the calibration and errors on Fourier coefficients.

From both calibration measurements we obtained the parameters and the errors as seen in Tab. 3.10

δ	86.89 ± 0.23°
α_0	-3.84 ± 1.00°
β_0	18.66 ± 0.50°

Table 3.10: Results from calibration procedure

With the method described in section 2.7 we obtain following results for measurements with different polarizations, as shown in Tab. 3.11. A comparison between measured intensity and simulated intensity from eq. (3.24) with the calculated Fourier coefficients is shown in Fig. 3.21.

	$\frac{M}{I}$	$\frac{C}{I}$	$\frac{S_1}{I}$	$\frac{S_2}{I}$	$\frac{\lvert S\rvert}{I}$	$\frac{\lvert M\rvert}{I}$	$\frac{L}{I}$
H-light	1.058 ± 0.064	-0.171 ± 0.013	0.042 ± 0.003	0.111 ± 0.006	0.084 ± 0.002	1.072 ± 0.010	1.072 ± 0.010
H-light exp	1.000	−0.002			0.005		1.000
V-light	-0.689 ± 0.053	0.934 ± 0.071	0.056 ± 0.005	-0.026 ± 0.003	0.044 ± 0.003	1.161 ± 0.054	1.161 ± 0.054
V-light exp	−1.000	0.005			−0.003		1.000
RC-light	0.035 ± 0.004	-0.076 ± 0.007	1.415 ± 0.074	-0.079 ± 0.005	1.004 ± 0.005	0.084 ± 0.004	0.084 ± 0.004
RC-light exp	0.124	0.013			0.992		0.124
E-light	0.218 ± 0.016	-0.722 ± 0.052	0.838 ± 0.054	-0.210 ± 0.014	0.612 ± 0.023	0.754 ± 0.029	0.754 ± 0.029
E-light exp	0.530	0.615			0.583		0.811

Table 3.11: Result from measurement of the Stokes parameters with the self-calibrating polarimetric method

The relative errors on $\frac{S}{I}$ for all measurements are less than 7%. For $\frac{M}{I}$ and $\frac{C}{I}$ they are mostly below 10%, except where the Stokes parameters are near zero. For $\frac{L}{I}$ we have relative errors around 5%.

Uncertainties arise from intensity fluctuations, finite precision in the rotation of the motorized wheel, and finite precision in setting the angles of the linear polarizer for the two measurements at $\alpha_0 = 0°$ and $\alpha_0 = 45°$.

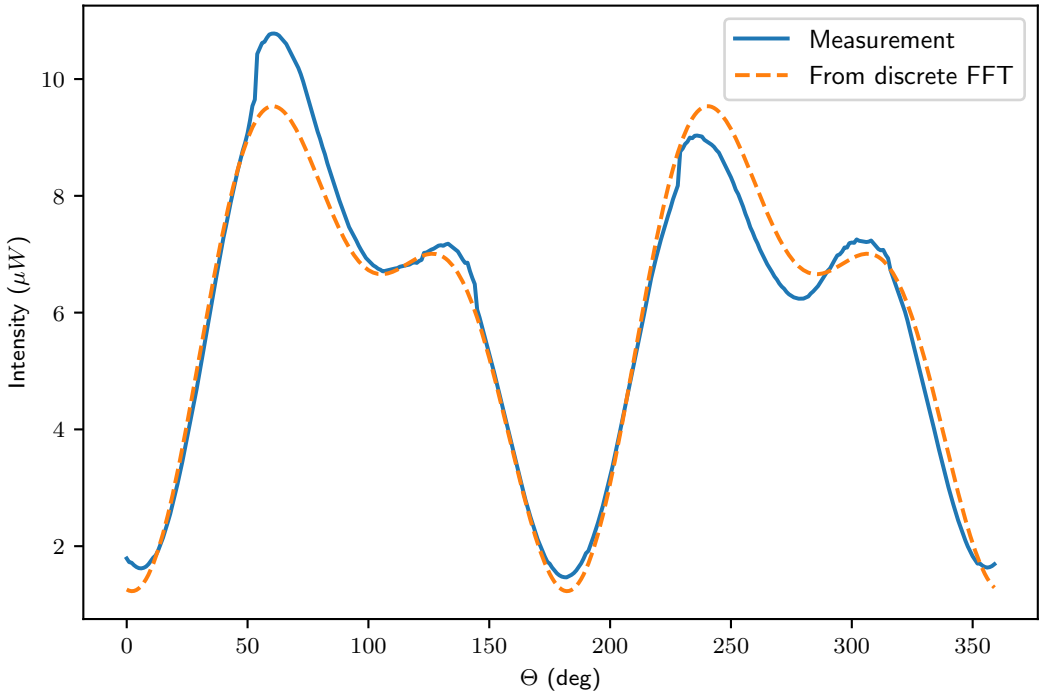

Figure 3.21: Solid curve shows the intensity measurement for elliptical light with M=0.530, C=0.615, S=0.583, dashed curve shows the intensity calculated from the determined Fourier coefficients for the self-calibrating polarimetric method

The results indicate that the self-calibrating polarimetric method works, as the most measured values are close to the expectations. As the Stokes parameters are added in square to unity a remaining circular polarization of around 0.1 means that the light is still nearly fully linearly polarized. For nearly all Stokes parameters, except $\frac{|S|}{I}$ and $\frac{L}{I}$, the main contribution to the uncertainty comes from the angles α_0, $\tilde{\alpha}$, and β_0. For $\frac{|S|}{I}$ and $\frac{L}{I}$ the errors from the angles and the intensity are equally important. Thus, by setting up the calibration angles with better precision than $\pm 1°$, it is possible to effectively reduce the uncertainties in the Stokes parameters. Then the next step in improving accuracy should be reduction of laser intensity fluctuations below $\pm 1\%$. This can be achieved by splitting the laser light into two beams and observing the intensity fluctuations of the second beam. Usually, there is a coherence between these two and the fluctuations can be removed, e.g by dividing by the intensity of the second beam [11].

The expressions for $\frac{C}{I}$, $\frac{S_1}{I}$ and $\frac{S_2}{I}$ do not seem to be very robust compared to the expected values, so it is advisable to consider mainly the expressions $\frac{|S|}{I}$ and $\frac{L}{I}$ in order to determine the state of circular and linear polarization. Another possible source of error is the non-perpendicularity of the quarter-waveplate to the rotation axis, which causes the laser beam to hit the detector at different points of the surface and possibly introduces fluctuations in the intensity if the detectors sensitivity is not uniform. Further the non-perpendicularity of the laser beam to the quarter-waveplate leads to a different retardance δ than determined by the calibration, as the light travels varying distances within the waveplate. This error could easily be reduced by installing a high precision angular mount for the rotating wheel improving the repeatability of the measurements.

3.5.2.3 Comparing monochromatic to achromatic waveplates

The achromatic waveplate SAQWP05M-1700 from Thorlabs has according to the manufacturer a flat retardance over a broad spectal range [17], but it shows an angular dependence of the transmitted intensity known as waveplate ripple. The plate itself consists of 6 optically cemented plates of which 3 are made of quartz and three of MgF_2 after a design from Pancharatnam [18], which makes the retardance uniform for a wide spectral range when the birefringent crystals are combined at the correct orientations. We compared the achromatic waveplate to an monochromatic waveplate by doing a full rotation in the rotating wheel for each of them and observing the angular dependence of the transmitted intensity. We used the self-calibrating polarimetric method to investigate how the calculated intensity from the Fourier coefficients behaves in comparison to the measured intensity.

The results in Fig. 3.22 and Fig. 3.23 showed that the modulation of the transmitted intensity during the rotation is much more prominent in the achromatic waveplate than in the monochromatic waveplate.

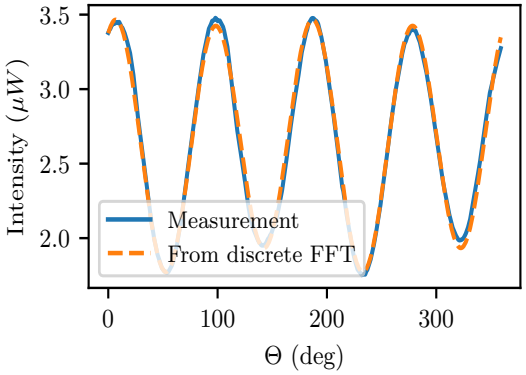

Figure 3.22: Measured intensity and calculated intensity from Fourier coefficents for a monochromatic $\frac{\lambda}{4}$-waveplate $\lambda = 633$nm

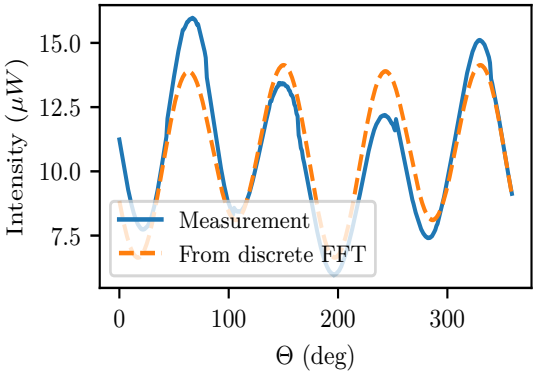

Figure 3.23: Measured intensity and calculated intensity from Fourier coefficents for achromatic $\frac{\lambda}{4}$-waveplate 600-2700 nm

The maximum amplitudes for the monochromatic case were nearly constant, whereas the maximum amplitudes for the achromatic case showed a much stronger modulation about 10 % of the expected peaks.

The angular modulation comes from multiple reflections within the plates, where the initially transmitted light shows a phase shift of $\frac{\pi}{2}$ between ordinary (o) and extraordinary (e) light rays. For multiple reflections the e and o rays show a phase shift of π. The different beams are out of phase, which leads to an angular intensity modulation similar to a Fabry-Pérot interferometer [14]. This leads to a behaviour of the achromatic quarterwaveplate, which noticeably deviates from an ideal one.

There are a few options how to take into account this modulation when calculating Stokes parameters. The easiest way would be to use a monochromatic waveplate, but this collides with our task to build a polarimeter for a wide spectral range. We could also rotate the waveplate by 180°, take another measurement and average it with the measurement taken at 0°, which effectively would cancel the ripple out. For our methods employing Fourier transformations we actually can disregard the ripple, as we only consider modulations of the frequencies 2ω and 4ω for our calculations of the Stokes parameters, whereas the ripple modulation has a frequency of ω. The fact that we can repeat the calculation using the method by Andreev with the averaged intensity, where the ripple is eliminated and still obtain the exact same Stokes parameters strengthens this assumption. A similar approach

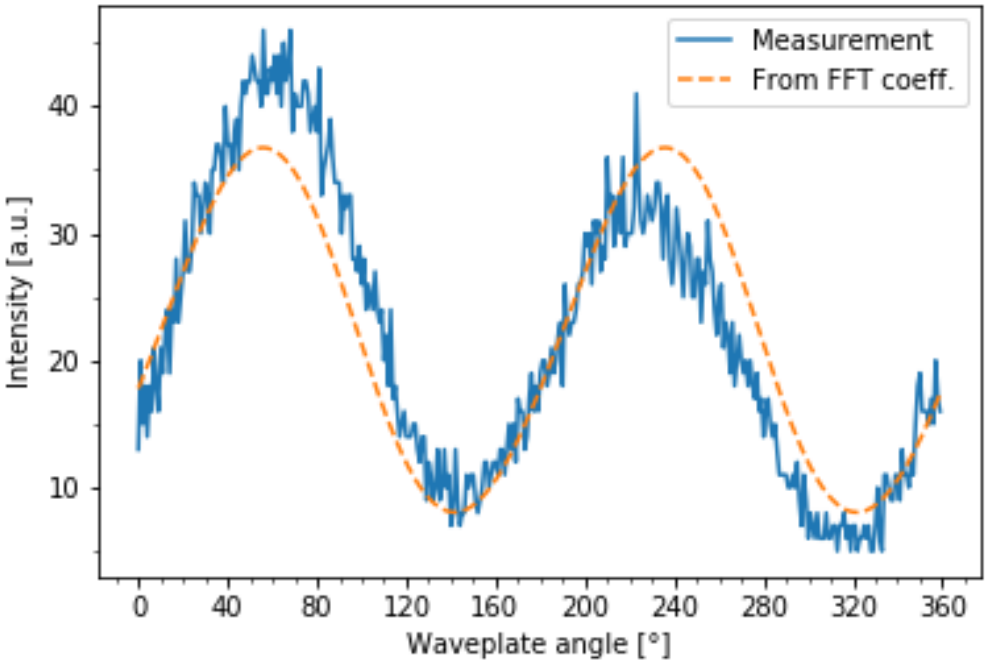

Figure 3.24: Angular dependence of intensity of trion peak with the background subtracted for WSe_2 monolayer excited with LC-light at 1.710 eV

was taken by Adamson, where the ripple in the linear Stokes parameters recorded by an infrared telescope was removed by cutting out the affected Fourier components [19].

3.5.3 Test on photoluminescence emission from a WSe_2 monolayer

A WSe_2 monolayer was placed into a cryostat and cooled down to 14 K. Then the laser beam of a Sirah Matisse TR 692 nm cw laser was focused onto the sample. After calibrating and focusing the laser beam the train consisting of the linear polarizer LP2, the half-waveplate 600-2700 nm and the quarter-waveplate 690-1200 nm was inserted into the laserbeam. The now polarized laser light hit the sample and excited the material.

The photoluminescence signal from the sample, which was guided through the rotating plate polarization measurement setup was ultimately detected in a spectrometer (Andor Shamrock). Intensity measurements depending on the rotating plate angle were recorded and spectrally resolved.

The sample was excited with four different polarizations, namely H-, V-, LC-, and RC-light. The data was loaded into the program Py2DSpectroscopy by Sven Borghardt, where the data could be depicted spectrally and an angular dependence of the intensity for each energy could be shown as well, see Fig. 3.24. For each spectrum 3 prominent peaks, namely Exciton, Dark Exciton and Trion peaks as depicted in Fig. 3.25 were further analyzed for their polarization. Therefore, after subtracting the background, for each peak the mean energy was estimated and within a width of 10 meV each discrete energy was subjected to a polarization analysis by regarding angular dependence of the intensity for a particular energy. Usually the energy with the most counts within a peak was chosen as representative.

From both calibration measurements we obtained the parameters and the errors as seen in Table 3.12

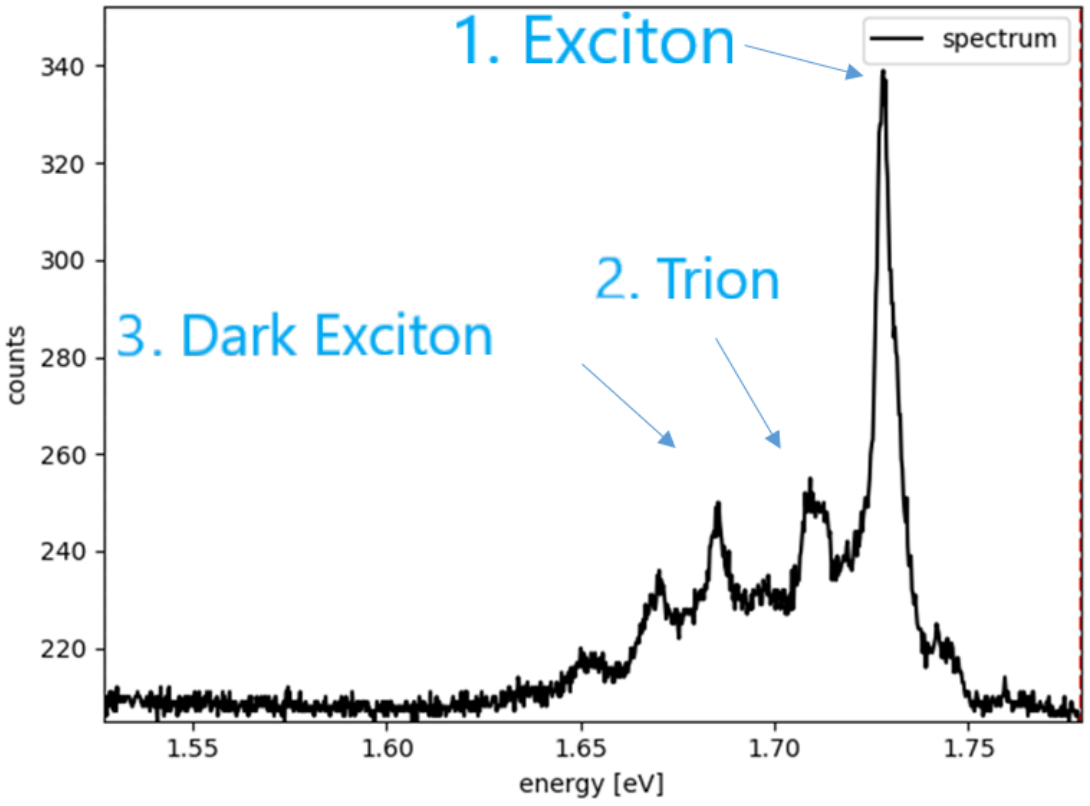

Figure 3.25: Spectrum of WSe_2 monolayer excited with LC-light.

δ	88.40 ± 0.47°
α_0	-22.53 ± 1.03°
β_0	-7.99 ± 0.53°

Table 3.12: Results from calibration procedure for excitons in monolayer measurement

We found that in general peak 2, which corresponds to a trion, has the strongest response to excitation with light of a particular polarization. It showed the same partial polarization to a degree of typically 40-60 % as seen in Tab. 3.13 and Tab. 3.14, except for excitation with H and V-light, where it responded with a mix of horizontal and diagonal polarization, see Tab. 3.15. But grouping H- and V- light together to linear polarization we return to a partial polarization in the range 40-60 %. The other two peaks responded to the excitation in a similar way with a partial polarization of 20%. As the peaks had a width of 10 meV the energies off from the center were also subjected to a polarization analysis, but going to the edge of the peaks the DOP became gradually smaller, until unpolarized wavelengths were reached.

We saw that various excitons react in different degrees of partial polarization to the excitation with laser light, so the kind of exciton can be coarsely determined employing this method. Trions can be detected if the monolayer emits light with 40-60 % of the same polarization it was illuminated with. The errors on the Stokes parameters are not higher than 6%. We expect trions to conserve only circularly polarized light to a certain degree, so the measurement does not correspond too well with our expectations, as linearly polarized light is conserved approximately to the same degree. Excitons and dark excitons show the same general behaviour, but their returned degree of polarization is lower, about 20% with similar errors on the Stokes parameters as for the trions. Thus, it is hard to

differentiate excitons and dark excitons just from the returned DOP. We expect excitons to retain linearly and circularly polarized light to a certain degree, so the measurement agrees with our expectations. We expect dark excitons to be unpolarized in general, but due to a non-ideal setup linear polarization is often present, which is also true for our measured values. If we excite the dark exciton with circularly polarized light we see a response with circularly polarized light, which is not expected.

All this hints at a non-perfect calibration of our setup, e.g. from the compensator, which is supposed to cancel out the effects of the optical components placed between the cryostat and the polarimeter, so further experiments would be necessary to localize the exact error source.

	$\frac{M}{I}$	$\frac{C}{I}$	$\frac{S_1}{I}$	$\frac{S_2}{I}$	$\frac{\lvert S\rvert}{I}$	$\frac{\lvert M\rvert}{I}$	$\frac{\lvert L\rvert}{I}$
Excitation light	0.01	0.003			−0.999		
Peak 1 Exciton	0.020 ± 0.003	0.019 ± 0.001	0.151 ± 0.002	-0.213 ± 0.005	-0.200 ± 0.008	0.001 ± 0.001	0.016 ± 0.001
Peak 2 Trion	0.018 ± 0.005	-0.054 ± 0.004	0.417 ± 0.006	-0.724 ± 0.020	-0.665 ± 0.001	0.057 ± 0.003	0.102 ± 0.003
Peak 3 Dark exciton	-0.228 ± 0.011	0.041 ± 0.002	0.178 ± 0.004	-0.238 ± 0.008	-0.226 ± 0.001	0.232 ± 0.002	0.184 ± 0.002

Table 3.13: Results for excitation with LC-light of a WSe_2 monolayer

	$\frac{M}{I}$	$\frac{C}{I}$	$\frac{S_1}{I}$	$\frac{S_2}{I}$	$\frac{\lvert S\rvert}{I}$	$\frac{\lvert M\rvert}{I}$	$\frac{\lvert L\rvert}{I}$
Excitation light	−0.002	0.004			1.000		
Peak 1 Exciton	0.020 ± 0.003	0.027 ± 0.001	0.065 ± 0.001	0.258 ± 0.007	0.228 ± 0.001	0.034 ± 0.001	0.017 ± 0.001
Peak 2 Trion	-0.012 ± 0.004	0.073 ± 0.002	0.133 ± 0.002	0.635 ± 0.018	0.559 ± 0.001	0.074 ± 0.002	0.054 ± 0.002
Peak 3 Dark exciton	-0.037 ± 0.005	0.204 ± 0.014	0.082 ± 0.001	0.218 ± 0.005	0.195 ± 0.001	0.207 ± 0.003	0.238 ± 0.003

Table 3.14: Results for excitation with RC-light of a WSe_2 monolayer

	$\frac{M}{I}$	$\frac{C}{I}$	$\frac{S_1}{I}$	$\frac{S_2}{I}$	$\frac{\lvert S\rvert}{I}$	$\frac{\lvert M\rvert}{I}$	$\frac{\lvert L\rvert}{I}$
Excitation light	1.000	−0.005			−0.002		
Peak 1 Exciton	0.226 ± 0.011	-0.125 ± 0.006	0.030 ± 0.001	0.017 ± 0.001	0.021 ± 0.001	0.258 ± 0.003	0.190 ± 0.003
Peak 2 Trion	0.448 ± 0.028	-0.255 ± 0.016	-0.008 ± 0.001	0.001 ± 0.001	-0.004 ± 0.001	0.516 ± 0.006	0.516 ± 0.007
Peak 3 Dark exciton	0.079 ± 0.005	0.239 ± 0.015	0.018 ± 0.001	-0.033 ± 0.001	-0.030 ± 0.001	0.252 ± 0.004	0.253 ± 0.004

Table 3.15: Results for excitation with H-light of a WSe_2 monolayer

	$\frac{M}{I}$	$\frac{C}{I}$	$\frac{S_1}{I}$	$\frac{S_2}{I}$	$\frac{\lvert S\rvert}{I}$	$\frac{\lvert M\rvert}{I}$	$\frac{\lvert L\rvert}{I}$
Excitation light	−1.000	0.002			0.002		
Peak 1 Exciton	-0.092 ± 0.004	0.181 ± 0.010	0.034 ± 0.001	-0.006 ± 0.001	0.017 ± 0.001	0.203 ± 0.003	0.169 ± 0.003
Peak 2 Trion	-0.240 ± 0.015	0.408 ± 0.025	-0.047 ± 0.001	-0.040 ± 0.001	-0.041 ± 0.001	0.474 ± 0.005	0.474 ± 0.005
Peak 3 Dark exciton	0.241 ± 0.015	0.189 ± 0.010	-0.044 ± 0.001	-0.054 ± 0.002	-0.052 ± 0.001	0.307 ± 0.005	0.282 ± 0.005

Table 3.16: Results for excitation with V-light of a WSe_2 monolayer

4. Conclusions

The objective of the thesis was to construct an automated quarter-waveplate polarimeter, which can sufficiently distinguish between different kinds of polarization and has spectral resolution. A crucial part for improving the precision of the measurement of the Stokes parameters was the determination of the retardance of the achromatic quarter-waveplate. The results showed that the method with the quarter-waveplate rotating between two linear polarizers and the method with the Müller-matrix fitting are limited in their applicability due to waveplate ripple. The self-calibrating polarimetric method turned out to be the most effective, as the waveplate ripple can be disregarded and the required calibration of the angles of the quarter-waveplate and linear polarizer are carried out with high accuracy. The application of this method to an exciton measurement in a monolayer material resulted in a determination of the Stokes parameters with an error around 6%. Thus, we can conclude that the method is suitable for further polarimetric experiments, as long as the requirements for the precision are not too high.

Bibliography

[1] G. Können, "Viewing our world with polarizing glasses", Endeavour **10**, 121–124 (1986).

[2] J. A. Norling, "Light Control by Polarization and the Application of Polarizers to the Stereoscopic Process", Journal of the Society of Motion Picture Engineers **48**, 129–144 (1947).

[3] Y. Bobrov, O. Kuchenkova, M. Kouznetsov, P. Lazarev, A. Manko, V. Nazarov, N. Ovchinnikova, M. Paukshto, P. Protsenko, and S. Remizov, "LCD applications of thin-crystal-film polarizers", Journal of the SID **12**, 125–133 (2004).

[4] J. L. Volakis, *Antenna Engineering Handbook*, Vol. 23 (June 2007).

[5] H. G. Park, C. C. Pohalski, and B. Y. Kim, "Optical Kerr switch using elliptical-core two-mode fiber", Opt. Lett. **13**, 776–778 (1988).

[6] S. Chandrasekhar and E. Fermi, "Magnetic Fields in Spiral Arms.", apj **118**, 113 (1953).

[7] R. E. Lyle and G. G. Lyle, "A brief history of polarimetry", Journal of Chemical Education **41**, 308 (1964).

[8] J. Hough, "Polarimetry: a powerful diagnostic tool in astronomy", Astronomy & Geophysics **47**, 3.31–3.35 (2006).

[9] A. T. Hanbicki, M. Currie, G. Kioseoglou, C. S. Hellberg, A. L. Friedman, and B. T. Jonker, "Optical polarization of excitons and trions under continuous and pulsed excitation in single layers of WSe2", Nanoscale **9**, 17422–17428 (2017).

[10] W. A. Shurcliff, *Polarized Light* (Harvard University Press, City, 1962).

[11] D. Clarke, *Polarized light and optical measurement* (Pergamon Press, Oxford New York, 1971).

[12] V. Andreev, C. D. Panda, P. W. Hess, B. Spaun, and G. Gabrielse, "A self-calibrating polarimeter to measure Stokes parameters", arXiv e-prints, arXiv:1703.00963, arXiv:1703.00963 (2017).

[13] *Operation Manual Polarization Analyzing System PAX5710*, `https://www.thorlabs.com/drawings/804f29345fb21f2f-7DC2C8D0-03C5-D8CB-0EB0D99C0B5ABF29/PAX5710VIS-T-Manual.pdf`.

[14] D. K. Aitken and J. H. Hough, "Spectral Modulation, or Ripple, in Retardation Plates for Linear and Circular Polarization", Publications of the Astronomical Society of the Pacific **113**, 1300–1305 (2001).

[15] H. G. Berry, G. Gabrielse, and A. E. Livingston, "Measurement of the Stokes parameters of light", Appl. Opt. **16**, 3200–3205 (1977).

[16] *PRM1Z8 Motorized Rotation Stage User Guide*, `https://www.thorlabs.com/drawings/1c5e1bba984e75a3-3C98F070-A323-B162-1AD59ED2AD741B44/PRM1_MZ8-Manual.pdf`.

[17] T. Inc, *Superachromatic waveplates description*, (2019) `https://www.thorlabs.com/newgrouppage9.cfm?objectgroup_id=2193` (visited on 07/23/2019).

[18]S. Pancharatnam, "Achromatic combinations of birefringent plates", Proceedings of the Indian Academy of Sciences - Section A **41**, 130–136 (1955).

[19]A. J. Adamson, D. C. B. Whittet, A. Chrysostomou, J. H. Hough, D. K. Aitken, G. S. Wright, and P. F. Roche, "Spectropolarimetric Constraints on the Nature of the 3.4 Micron Absorber in the Interstellar Medium", The Astrophysical Journal **512**, 224–229 (1999).